12-2001

The Relationship between Rheology, Application Method, and Final Coating Structure

Basant Galal Dimetry

THE RELATIONSHIP BETWEEN RHEOLOGY, APPLICATION METHOD, AND FINAL COATING STRUCTURE

By

Basant Galal Dimetry

B. S. Georgia Southern University, 1998

A THESIS

Submitted in Partial Fulfillment of the

Requirements for the Degree of

Master of Science

(in Chemical Engineering)

The Graduate School

The University of Maine

December, 2001

Advisory Committee:

Douglas W. Bousfield, Professor of Chemical Engineering, Advisor

Adriaan R. P. van Heiningen, Professor of Chemical Engineering

Hemant P. Pendse, Professor of Chemical Engineering

THE RELATIONSHIP BETWEEN RHEOLOGY, APPLICATION METHOD, AND FINAL COATING STRUCTURE

By Basant Galal Dimetry

Thesis Advisor: Dr. Douglas W. Bousfield

An Abstract of the Thesis Presented
in Partial Fulfillment of the Requirements for the
Degree of Master of Science
(in Chemical Engineering)
December, 2001

Paper is coated to improve the printability and the visual properties. The factors that determine the coating structure are important because the structure determines the physical, optical, and printing properties. This work focuses on determining a relationship between the rheological properties of the coating, the application method, and the final coating structure. Coatings with different polymers and pigments were characterized in terms of steady shear and viscoelastic properties. These coatings were applied onto plastic film and paper with a laboratory rod coater, a spray coater, and a high-speed blade coater. The final coating structure after drying was characterized in terms of void fraction, water absorption rate, gloss, and light scattering coefficient.

A relationship between the viscoelasticity of the suspensions and the final coating structure was found for the associative thickeners. However, the

concentration and molecular weights of cellulosic thickeners did change the wet state rheology, but the final coating structure was not changed. Pigment shape, type, and size distribution are more important than the elastic modulus when predicting coating properties. For all coatings, a correlation is found between shear viscosity and gloss.

Application method has an influence on the final structure: the light scattering coefficient changed slightly, but spray coating gave lower gloss, larger absorption rates, and larger void volume compared to the blade coating and rod coating methods. This result was due to poor leveling and spreading of drops at low coat weights.

ACKNOWLEDGEMENTS

I would like to extend my utmost appreciation to my advisor Dr. Douglas W. Bousfield for his support and guidance throughout this project. I would also like to take the opportunity to thank my other committee members Dr. Adriaan R. P. van Heiningen, and Dr. Hemant P. Pendse for spending their time and energy for the benefit of my thesis.

This project would not have been possible without the technical and financial support of the industrial sponsors of the Paper Surface Science Program at the University of Maine, and I would like to thank them.

I must also thank the graduate students and staff of the Chemical Engineering Department of their support and encouragement throughout the last two years. A special thanks goes to Proserfina D. Bennett, Katharina Prall, and Seongnam Ahn for their invaluable guidance in the area of paper coating applications.

The opportunity to study at the University of Maine would not have been possible without the encouragement of my family, and to them I owe everything because they are my backbone.

Finally, this work is dedicated to my fiancé, Mark A. Paradis, for his support and encouragement through all of the good and bad moments.

TABLE OF CONTENTS

LIST OF TABLES

LIST OF FIGURES

1. INTRODUCTION

Coatings are used in many different industries for many different reasons. In the metal industry, coatings are used to protect metals from erosion. In the photography industry, precision coatings are used for making photographic film on magnetic media. In the paperboard industry, coatings are used to waterproof corrugated boards. In the ceiling tile industry, coatings are used for low gloss and noise absorption properties on the tiles. In the paper industry, coatings are used to improve the printability, the visual properties, and the functionality of the paper.

In the paper industry, researchers have great interest in the area of determining the dominating factors that influence the final coating structure. Nisogi *et al.* (1,2) showed that it might be possible to correlate the wet suspension with the final coating structure for a system containing an associative thickener. They found that as the polymer concentration increased, so did the elasticity of the suspension, and they found a relationship between the elasticity and void fraction and the light scattering coefficient.

1.1. Objectives

The objectives of this study are to understand the role of pigment and particle interactions on the final coating structure and to determine if application method has an affect on the final coating structure. To understand the role of the pigment and particle interactions, Figure 1.1 is a depiction of the coating layer on the substrate before and after drying without the presence of polymer and with

polymer present. This interaction is yet to be understood, and the depiction is only a hypothesis. When polymer is present, then perhaps the final coating bulk is more porous and more structured (Figure 1.1, d.) than when the polymer is not present (Figure 1.1, b.)

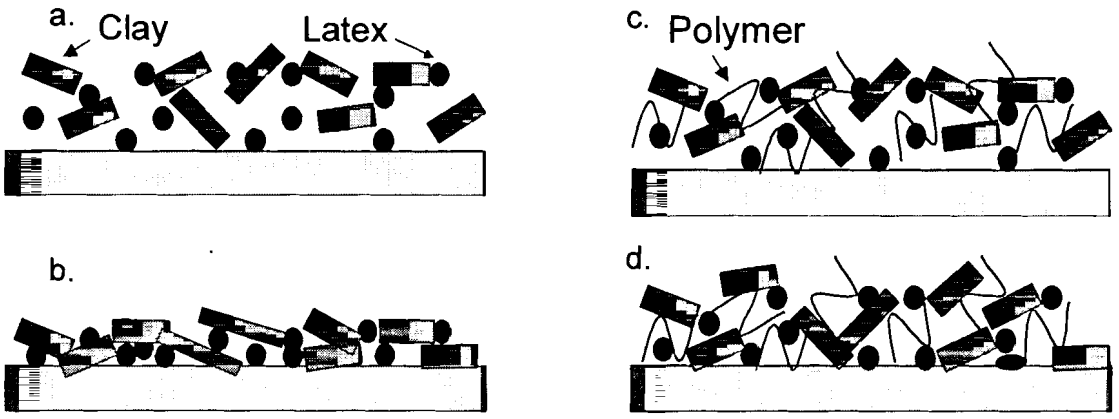

Figure 1.1 Particle/Polymer Interactions: a.) Clay and Latex Suspension as Applied with Water; b.) Upon Drying; c.) Clay, Latex, and Polymer as Applied with Water; d.) Upon Drying

To help determine these interactions, it would be beneficial to determine which polymers alter the final coating structure, and to determine whether the wet coating breaks down upon metering and if it does, to determine the rate of reformation of the structure or whether reformation occurs.

It is also interesting to determine whether application method alters the final coating structure as depicted in Figure 1.2. It is not clearly understood how the structure reforms after the coating is metered. The coating suspension may contain the polymers that are interacting with the clay and latex to form a network (Figure 1.2, a.). Upon metering, the shear may break down the network (Figure 1.2, b.). It is interesting to determine the conditions under which this

phenomenon may be happening. This depiction and phenomenon is only a hypothesis.

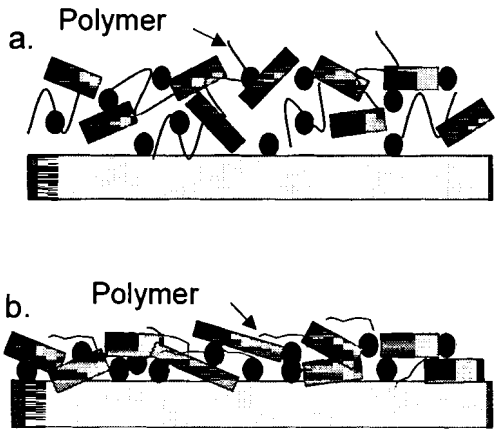

Figure 1.2 Particle/Polymer Interactions: a.) Clay, Latex, and Polymer as Applied with Water; b.) Upon Drying After Being Metered

1.2. Approach

To meet the objectives of this study, coating formulations were chosen to vary different aspects of the system. Several polymers of different molecular weights and of different particle association mechanisms were tested. Pigments were varied to test the effect of particle size and shape. The latex binder used in these formulations remained constant.

The rheology of the coating suspensions was characterized for steady shear and viscoelastic properties and elasticity. The coatings were then coated using a laboratory rod draw down coater, a cylindrical laboratory blade coater (CLC), and an internal-mixing air-assisted spray coater. The final coating structure was characterized for void fraction, water absorption, gloss and light scattering coefficient.

2. BACKGROUND

The understanding of coating structure, the spatial arrangement of pigment particles and binders, and what influences it is essential to control the quality of the coatings and to develop new products. The control of structure properties is well understood, but questions remain as to achieving the desired end-product properties of the coating layer. The rheology of coating suspensions has been studied, however the complexity of the suspension hinders a single parameter to describe the flow of the suspension during the coating process (3, 4).

2.1. Rheological Measurements

2.1.1. Theory

Rheology is a study of material deformation. The ease of deformation to a steady strain rate is known as *viscosity*. The degree of *elasticity* is the measure of the solid-like behavior or response to strain. Rheology and viscosity should not be confused since viscosity is the measure of the resistance to flow. The ability of a material to thin or thicken with increasing *stress*, or amount of force applied in the x-direction, and the point at which a material begins to flow, also known as the *yield stress* (5). There are generally two types of materials, Newtonian and non-Newtonian. *Newtonian materials* are characterized by constant viscosity over a large range of stress. Examples of Newtonian materials

include water, alcohol, and most oils. *Non-Newtonian materials* are defined by remarkable changes in the viscosity of suspensions with changes in stress. The major interests of rheology are the study of peculiar flow characteristics of non-Newtonian materials and the study of concentrated suspensions.

Figure 2.1 (5) is a depiction of the velocity gradient created in a liquid between two parallel plates of area A. One plate is positioned at y = 0, and the other is positioned at y = d. The plate at y = d is moved at a relative velocity U while the plate at position y = 0 remains stationery. The force F exerted on the liquid creates a velocity gradient where the small arrows are proportional to the local velocity. This motion creates internal friction. The resistance to this force is the *shear viscosity*. *Shear strain* is described as "the movement of a layer of material relative to parallel adjacent layers" (5), and is generally referred to as *shear*. The change in shear strain per unit time, known as the *shear rate* $\dot{\gamma}$, creates the velocity gradient. The force parallel to the plate at y = d is known as the *shear stress* σ. Steady shear measurements are traditionally regarded as the most important material properties that result in the knowledge of the material response.

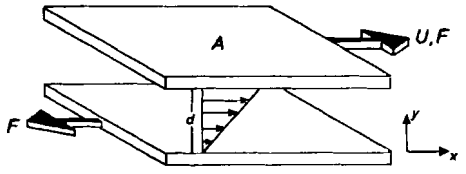

Figure 2.1 Velocity Gradient Created by Parallel Plates Being Moved at Velocity U in the x-Direction for Simple Shear Flow (5)

For non-Newtonian materials, the shear viscosity η is the shear stress σ_{yx} as related to the velocity gradient, or shear rate $\dot{\gamma}$, and can be express as

$$\eta\left(\dot{\gamma}\right) = \frac{\sigma_{yx}}{\dot{\gamma}} \tag{2.1}$$

Non-Newtonian suspensions exhibit elastic properties as well as viscous properties. Some exhibit properties of a viscous fluid and an elastic solid. These particular characteristics are known as *viscoelasticity*. Elasticity describes the ability to store mechanical energy reversibly during deformation (6). Viscoelastic properties are attributed to the breakdown and reformation of the network structure of applied shear stress.

Linear viscoelasticity is based on the superposition principle that implies that the strain at any time is directly proportional to the stress (5). For linear viscoelasticity, the differential equations are linear, and the coefficients of time and the material parameters are constant. For investigating linear viscoelasticity, small amplitude oscillatory shear flow is the most common deformation mode. For this type of deformation, one plate remains stationery while the other plate oscillates back and forth in the x-direction with small amplitudes. Different models exist to calculate the oscillatory shear rate, but for the purpose of this discussion, the Maxwell model will be used. For this case, the shear strain can be defined as

$$\gamma = \gamma_0 \cos(\omega t) \tag{2.2}$$

where $i = -1^{1/2}$, ω is the frequency, γ_0 is the strain amplitude, and t' is the initial time (5).

From equation (2.2), a *complex shear modulus* G^* can also be defined as

$$G^*(\omega) = i\omega \int_0^\infty \phi(\xi)\exp(-i\omega\xi)d\xi \tag{2.3}$$

where ξ represents the time scale (t - t') of the rheological history and ϕ represents the *relaxation function* based on the *relaxation time* τ, that is the time it takes "for the shear rate of the fluid to reduce to 1/e of its original equilibrium value" once the shear flow stops (5). G^* can also be written as

$$G^* = G'+iG'' \tag{2.4}$$

where G' is the *storage modulus*, or dynamic rigidity, and G" is the loss modulus, or the imaginary part of the complex shear modulus. G' is defined as being the part of the stress that is in phase with the strain divided by the strain under sinusoidal conditions, where as G" is the part of the stress that is out of phase with the strain. In other words, G' can by written as

$$G' = \frac{\eta\tau\omega^2}{1+\omega^2\tau^2} \tag{2.5}$$

and G" can be written as

$$G'' = \frac{\eta\omega^2}{1+\omega^2\tau^2} \tag{2.6}$$

From the equations defined, the shear stress can be written as

$$\sigma(t) = G^*\gamma(t) \tag{2.7}$$

and the *phase angle*, "the phase difference between the stress and strain in oscillatory deformation" (5), can be defined as

$$\tan\delta = \frac{G''}{G'} \tag{2.8}$$

To understand how the phase angle relates to the storage modulus and the loss modulus, Figure 2.2 graphically illustrates the oscillatory strain input and stress output for the viscoelastic region. The difference between the two curves is $\delta/2\pi$.

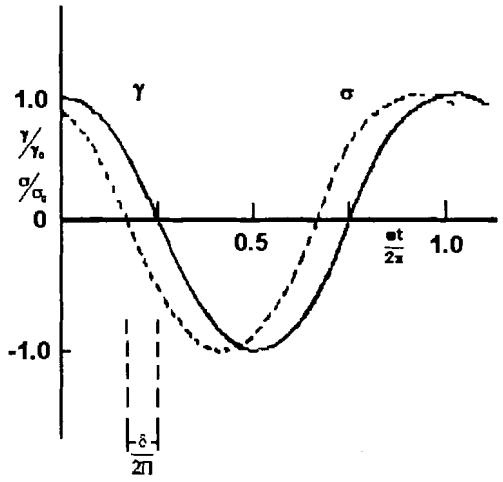

Figure 2.2 Wave Form of Oscillatory Strain Input and Stress Output (5)

2.1.2. Rheology of Coating Suspensions

Coating suspensions can be described in terms of viscoelastic properties. At low shear rates, the flow of these concentrated suspensions is described by solid-like behavior and possesses a *yield stress* σ_y (4), or a stress that must be overcome to move from an inelastic state to an elastic state, defined as

$$\sigma = \sigma_y + \eta\dot{\gamma} \tag{2.9}$$

Due to the highly concentrated coating suspensions, aggregates and flocs may be present if the solids are not evenly distributed forming a network that could change as forces on the system change. Along with many other works (7, 8, 12, 13), Nisogi *et al.* (1, 2) studied this affect as a function of changing the concentration of the cobinder present in the system as well as changing the solids content of the suspension. Kokko *et al.* (64) studied this affect on the macroscopic coating structure as a function of physical and chemical modifications to a styrene-butadiene latex binder.

2.2. Rheological Influences on Runnability and Coating Processes

Before the discussion of the importance of coating rheology on coating runnability, the term "runnability" must first be defined. In recent years, many researchers have defined runnability to be different things. Some have defined it to be the minimum coating speed on the cylindrical laboratory coater (CLC) at which wet streaks begin to appear (9), or the blade pressure on the coater (10). While others have defined it as the coat weight developed on a CLC and as the blade pressure on a short dwell pilot coater (11). All of these phenomena are encompassed in the definition of runnability, so it is important to determine the rheological dependence of these occurrences, yet no one rheological measurement can predict all of them at the same time (3, 4).

It has been shown that the rheology of the coating suspension influences the coating performance at high speeds (12, 13). The quality of the coated and printed papers is also affected by the rheology of the suspension (14).

Triantafillopoulos *et al.* (15) have shown that the viscoelastic properties affect the performance and runnability of the coating during blade coating, and in another study, he showed that low-shear viscosity and yield stress are the cause of short-dwell streaking (16). This was explained by the contribution of hydrodynamic instability in the flow before passage under the blade. The elastic component has been shown to become negligible compared to the viscous component at shear rates on the order of 10^6 s^{-1} (17).

Most of the work done to date has studied coating rheology and runnability as related to high-speed coating for blade coaters. A good understanding of the rheology and runnability of other coating methods is not clearly understood.

2.3. Factors Influencing Coating Structure

Coating structure is influenced by many different aspects such as the coating composition, the type and level of latex or other binders used (18), the pigment shape and size distribution (19), and the basesheet properties (42), and consolidation upon drying (19).

The structure forms upon consolidation by dewatering. The mechanism for consolidation was proposed by Watanabe *et al.* (18). They found that consolidation is influenced by the latex stiffness and colloidal interactions. A first critical concentration (FCC) was determined as the point at which the "immobilization solids" are reached, and a second critical concentration (SCC) was determined as the point of "true immobilization". It was determined that the network becomes fixed before the SCC is reached, and binder migration can be controlled between the FCC and the SCC to control the network formation.

On non-porous substrates, the amount of latex used influences the consolidation process (22). The consolidation of the coating is greatly influenced by the pigment packing when the level of latex is below the critical content for the system. The packing of the clay is very disordered. When the level of the latex is more proportional to the level on clay, then consolidation is dominated by the coalescence and the flow of latex upon drying. The structure becomes more orderly.

On paper, dewatering occurs to make way for consolidation by several processes (19). Pressure filtration takes place at the nip of the applicator roll. Capillary movement is a result of curved interfaces that create capillary pressure, as defined by the Washburn equation, so that dewatering increase as the moisture content of the paper decreases. Molecular sorption is the opposite effect of capillary movement and occurs as the moisture or the temperature of the paper increase. Spreading happens as the water spreads over the fiber surfaces leaving the pigment particles behind to form filter cakes. Evaporation also occurs when the temperature of the paper is increased.

2.4. Colloidal Interactions

Colloidal interactions may be the most important factor that influences the rheology and coating structure formation (19). Dispersion stability depends on the balance of van der Waals interactions and electrostatic repulsion. Pigment-pigment and pigment-binder interactions within the dispersion can be controlled by adjusting the pH (20, 21), the electrolyte content (20, 21), stabilizer concentration (22), amount of dispersant (23), desorption of stabilizers and

dispersants (24), addition of cationic polyelectrolytes (25, 26, 27), or amphoteric protein derivatives (28).

Pigment-binder interactions and pigment-pigment interactions help determine the structure of the suspension along with the rheology of the suspension (19). Despite the charge of the latex or other binders used (29), the interactions may be weak, as in the case of carboxymethyl cellulose (CMC) (30, 31), or they may be strong, as in the case of polyvinyl alcohol (PVA) (32, 31). Colloidal interactions also reduce the repulsive forces keeping the suspension dispersed. These forces help achieve lower *first critical concentration* (FCC), the first sudden change in opacity and gloss, values that in turn, yield higher void volumes in the coating layer producing smoother coatings (25, 26, 27, 28). The FCC values can be lowered by the extent of pigment-latex interactions and pigment-cobinder interactions. For example, the addition of CMC and PVA lower the FCC (33).

2.5. Coating Structure Characterization

The optical, mechanical, and absorption properties of paper are influenced by the porosity of the paper. Characterization of porosity, or air entrapment better know as voids, is encompassed by the understanding of the refractive index that influences the light scattering efficiency, the understanding of the interactions between pigment and surfaces that control coating adhesion and coating strength, and the rate of absorption at the liquid-solid interface (19).

Unique cross-sectional imaging of the porous network of a binder-free coating on plastic film was analyzed by Climpson and Taylor (34) who characterized voids as flattened spheres. Before this study, voids were generally characterized using mercury porosimetry. The strength of the binder-containing coating was found to be inversely proportional to the porosity of the coating (35). Others have characterized porosity by other techniques such as the silicon oil absorption technique (36).

The characterization of coating surface structure is obtained by gloss measurements as well as absorption measurements. It has been determined that the "macroscopic" gloss of the coating increases as a function of coat weight as the surface roughness decreases. This phenomenon reaches a leveling point that corresponds to the "microscopic" gloss of the particles (37, 38). When the absorption of the coatings was studied, it was determined that surface roughness was the determining factor in the rate of absorption (39, 40). The pores that form the solid-air interface in the coating structure were determined to be the light scattering species instead of the pigments as predicted by Alince *et al.* (20), Trader (41), and Hemstock *et al.* (23).

2.6. Coating Formulations

Coatings consist of pigments, binders, and additives. Coating formulations are based on pigment concentration. Pigments tint or color and enhance brightness of the coating. The most common pigments used are kaolin clay, calcium carbonate, titanium dioxide, and alumina trihydrate. Binders are used for binding pigments in the coating and coating to the paper fibers, and the

most common binders are natural binders, such as starch, soy protein, casein, and synthetic binders, such as latexes and polyvinyl alcohol. Additives encompass a large variety of products each used to perform a specific function, such as dispersants, viscosity modifiers, lubricants, cross-linkers, biocides, pH controllers, repellents, optical brighteners, dyes, and foam control agents (42).

When making a coating formulation, the order of addition is important to make certain that all the components are best utilized. The water and pigments should be mixed together first, then, in the following order, dispersants, cross-linkers, lubricants, anti-foam agents, binders (natural then synthetic), rheology modifiers, and finally optical modifiers should be added (42).

2.7. Coating Methods

Coating methods commonly used in the paper industry include blade coaters, rod coaters, air knife coaters, transfer roll coaters, cast coaters, and curtain coaters. Recently, spray coaters have become a new method to coat paper. For this study, blade coating, rod coating, and spray coating were tested.

Different aspects of these coating methods have been studied. To name a few aspects studied for blade coaters, blade streaking (43,44), roll deformation (45), shear rates (46), and particle motion (47) have been characterized. Wire-wound rod coaters have been studied for coating defects (48) and coating quality compared to smooth rods (49). In recent years, spray coating has found its way into dispersion coating as a low impact, non-contact means of coating low coat weight paper (50,51). Although a numerous amount of work has been performed

to obtain a better understanding of application methods, the impact of these different coating methods on the final coating structure is yet to be clearly understood.

The use of blade coating dates back to 1906 when the first patent was granted to Krouse and Baumann for the inverted-blade coating system. A patent granted to Trist in 1945 marked the real beginning for the industrial use of blade coating paper. Blade coating encompasses many application systems that include flooded nip coaters, short dwell coaters, puddle-type applicators, and two stream coaters (42).

The cylindrical laboratory blade coater used for this study utilizes the short dwell application system. It operates on the principle that the time period when the coating is in contact with the paper is short before a trailing blade removes the excess coating. Figure 2.3 is a depiction of an industrial scale short dwell coater. A pressurized pond located before the blade supplies the coating. For uniform coat weight, the coating is supplied through a series of pressurized orifices to ensure even coating pressures across the web. The excess coating passes through a final orifice which has an adjustable gap that affects the coating pressure against the web. The coating is also supplied by variable-speed pumps that also control the coating pressure. Since the coating supplied is pressurized, low blade pressure is required to remove the excess coating because there is less amount of coating penetration into the web (42).

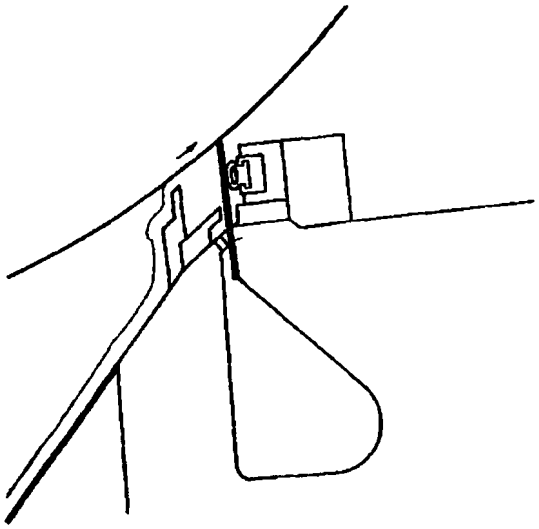

Figure 2.3 Short Dwell Coater (42)

Wire-wound rod coating began in 1905 when Charles W. Mayer founded the Mayer Coating Machines Company in Rochester, N. Y. This company began with the manufacturing of equalizer bars, rods made of carbon steel wound with music wire, for the carbon and wax paper industry. By the 1980s, other companies emerged, and the wire-wound rod evolved into a stainless steel rod and wire with closer tolerances and smoother finishes to sustain most coating materials and solvents used (52).

The coating is metered in the same manner as blade coaters. An excess amount of coating is applied to the web before the excess is removed by the rod. Figure 2.4 is a schematic of an on-line rod coater. This figure shows the web of paper being fed over an application roll that applies the excess coating before it is fed over the wire-wound rod for metering. The biggest difference in these metering methods is that when using a blade, coat weight is controlled by blade pressure, but when using a wire-wound rod, the coat weight is controlled by the amount of coating in the space between the wire coils (42,52).

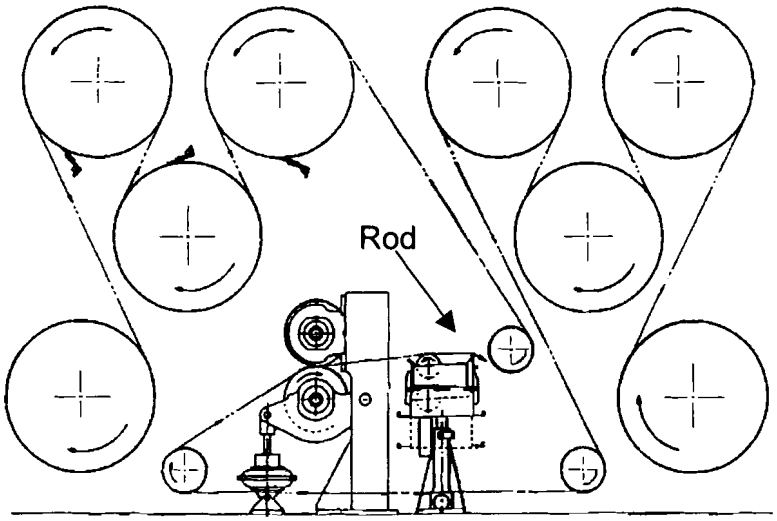

Figure 2.4 On-Line Rod Coater (42)

Spray coaters are used in number of different industrial processes such as combustion processes, spray drying and spray painting, and crop spraying to name a few (53). In 2001, spray coating found its way into the paper industry with the commercialization of the OptiSpray from Valmet. It is based on the principle of liquid atomization, which is the disintegration of a liquid jet into small droplets. This non-contact coating method does not use a separate metering device making it possible to use weaker webs that originate from recycled pulp (51).

Figure 2.5 is the commercially available OptiSpray Coater, but for the purpose of this study, a spray gun, similar to those used in the automotive industry for spray painting, was used. Spray guns are available using different atomizers such as pressure, air-assist, and airblast atomizers. Pressure atomizers are based on the concept of converting pressure into kinetic energy to produce a high relative velocity between the liquid and the surrounding gas. Air-

assist and airblast atomizers work on the concept that the kinetic energy of the air stream breaks the fluid jet or sheet into ligaments then into drops (53).

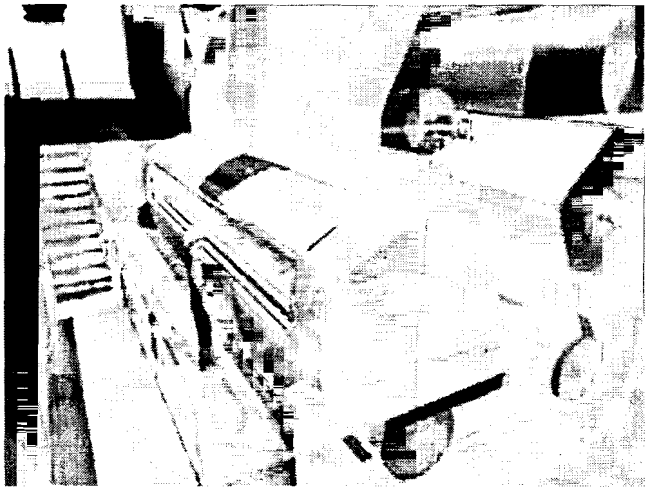

Figure 2.5 The On-Line OptiSpray Coater, 9.5 Meters in Length (51)

The spray gun used for this study is shown in Figure 2.6 with a pressurized quart-size sample cup. It is the Binks Model 95 Signature Series internal mixing air-assisted spray gun with a fan shaped nozzle.

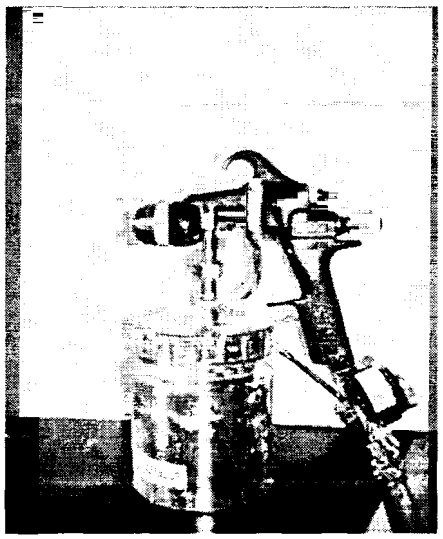

Figure 2.6 Binks Model 95 Signature Series Shown with Pressurized Sample Cup

3. EXPERIMENTAL METHODOLOGY

3.1. Materials

A simple coating suspension of delaminated kaolin clay (Covergloss, Huber, Lot #HBR110155171) was used with styrene butadiene latex (Dow, CP 620NA BK, Lot #NL10017213) as the basis for this study. Varying molecular weights of carboxymethylcellulose (CMC), were provided by Hercules, and the low molecular weight CMC at a concentration of 0.1 pph was used as the base line formulation for comparison with other polymers. For this particular study, the degree of substitution, DS, of 0.7 was used. All formulations contained 100 parts clay, 10 parts per hundred latex, and 60% solids by weight, and Table 3.1 shows the concentrations of CMC that were used along with the molecular weights studied.

Table 3.1 Carboxymethylcellulose

	Molecular weight (Daltons)	Concentration
Low:	120,000	0.1, 0.3, 0.5, 0.8 pph
Medium:	350,000	0.1 pph
High:	700,000	0.1 pph

The base line system was chosen to determine if the same correlations Nisogi *et al.* (1) found for the system of 100 parts of US #2 grade clay, 5 parts carboxylated styrene-butadiene latex, and a hydrophobically-modified alkali-swellable emulsion (HASE), a synthetic thickener, exist for other systems.

For the exploration of different aspects such as pigment type, particle size and distribution, and polymer type, other formulations of different pigments were used along with different polymers as can be seen in Table 3.2. The calcium carbonate (Albaglos S, particle size 0.6 μm) was provided by Specialty Minerals, and the plastic pigments (PP 723 and PP 755) were furnished by Dow Chemical. Hercules supplied the hydroxyethylcellulose (HEC) while the HASE and the hydrophobically-modified ethylene oxide-based urethane (HEUR) were supplied by Rohm and Haas.

Table 3.2 Other Formulations

Pigment	Polymer	Concentration
Medium Calcium Carbonate	Low MW CMC	0.1 pph
Plastic Pigment, 0.23 μm	Low MW CMC	0.3 pph
Plastic Pigment, 0.45 μm	Low MW CMC	0.1 pph
U. S. Grade #2 Kaolin Clay	Low MW CMC	0.3 pph
	HASE, RM 232	0.05, 0.5, 0.2 pph
Delaminated Kaolin Clay	HASE, RM 232	0.05, 0.1 pph
	HEUR, RM 12-W	0.1, 0.3, 0.5 pph

3.2. Coating Preparation

Dry pigments (kaolin clays) were dispersed in water at 72% solids by weight by using an overhead, dispersing mixer (Cowles Dissolver, Model W12), and the pH was adjusted to 9 using sodium hydroxide. The latex binder and polymers were added to the suspension and diluted with water to 60% solids by weight.

The calcium carbonate was used as slurry prepared by the manufacturer. The plastic pigments were also used as pre-dispersed slurry. These plastic pigments were provided at about 40% solids by weight; therefore, these coatings were prepared at 34% solids, which was equivalent to the pigment volume concentration of the other formulations.

The CMC was prepared according to recommendations from the supplier. It was dissolved in water by using two parts of an alcohol, (ethanol or methanol) as a co-solvent, to every one part of the polymer. It was used as a 3-4% solution in the coating formulations.

The HASE and HEUR are provided in an emulsion form. When using the HASE, the polymer was activated by adjusting the pH to 9, using sodium hydroxide, after the coating was prepared.

Polymer concentrations were varied, but the latex concentration remained constant for all formulations.

3.3. Rheology Experiments

The rheological measurements were previously determined by Nisogi. The Bohlin CVO (Bohlin Instruments), Figure 3.1, a constant shear rheometer with a 4°, 4 cm diameter cone and plate geometry (as seen in Figure 3.2), was used for all measurements (2).

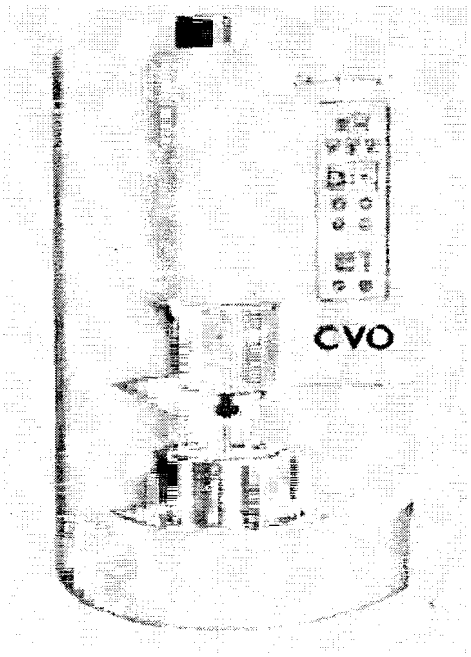

Figure 3.1 Bohlin CVO Rheometer

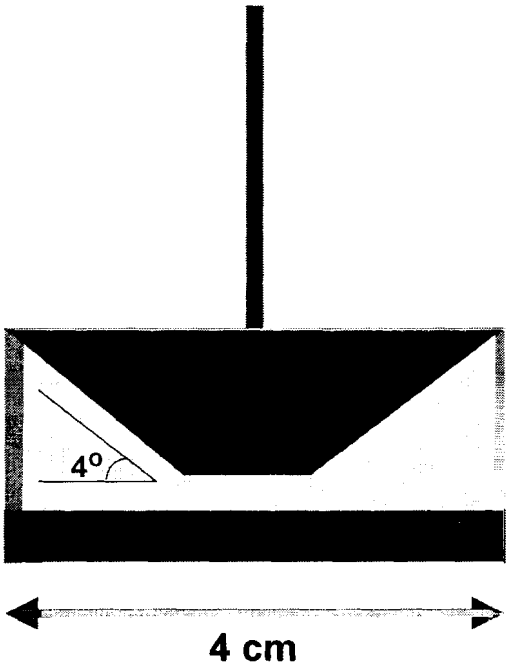

Figure 3.2 Bohlin CVO Geometry

3.3.1. Steady Shear and Viscoelastic Properties

The suspensions were characterized for their steady shear viscosity and viscoelastic properties. The steady shear viscosity was measured by increasing the amount of stress the samples. The parameters of this test very varied depending on the viscosity of each sample to produce a curve for shear rates ranging from 10 s^{-1} to 300 s^{-1}. This test also helped determine the stress required to shear the samples at 300 s^{-1} for further rheological testing.

Viscoelastic properties were measured for all suspensions over a range of 0.5 to 5 Hz to determine the linear viscoelastic region, discussed in Section 0, and to characterize the complex modulus, G*.

3.3.2. Steady Shear and Viscoelastic Properties

The suspensions were characterized for their steady shear viscosity and viscoelastic properties. The steady shear viscosity was measured by increasing the amount of stress the samples. The parameters of this test very varied depending on the viscosity of each sample to produce a curve for shear rates ranging from 10 s^{-1} to 300 s^{-1}. This test also helped determine the stress required to shear the samples at 300 s^{-1} for further rheological testing.

Viscoelastic properties were measured for all suspensions over a range of 0.5 to 5 Hz to determine the linear viscoelastic region, discussed in Section 0, and to characterize the complex modulus, G*.

3.3.3. Linear Viscoelasticity

To determine the linear viscoelastic region, an oscillating strain sweep test was performed over a range of 0.5% to 100% strain. In the linear viscoelastic region, the storage modulus and the elastic modulus are independent of applied strain. The experiments were performed by subjecting the samples to a pre-shear of 300 s^{-1} for 10 s then were allowed to equilibrate for 180 s. This shear rate of 300 s^{-1} was determined to be the highest level of shear that could be obtained using the cone and plate geometry without loss of the sample. The time frame was determined to be sufficient for breaking any structure that may have been present between particles. This rest time was to guarantee that the samples were exposed to the same shear history. Figure 3.3 illustrates the linear

viscoelastic region. All other oscillatory measurements were performed at 1% strain to ensure that the experiments were in this region.

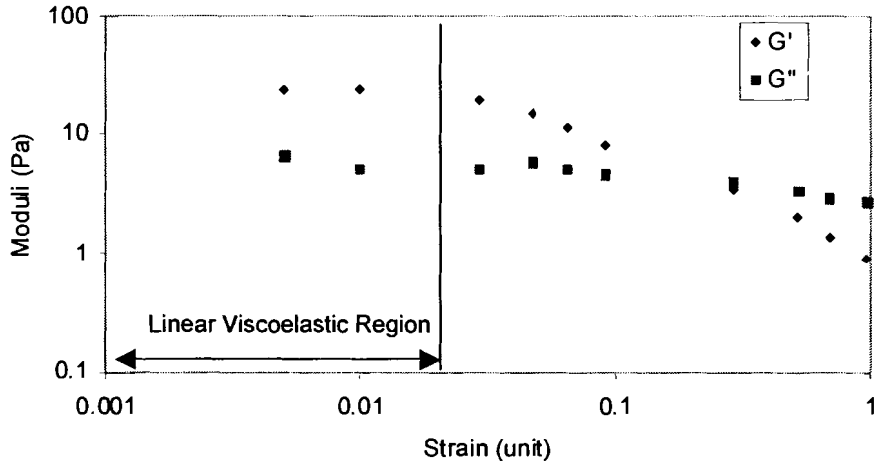

Figure 3.3 Linear Viscoelastic Region for Kaolin Clay Containing 0.1 pph Low Molecular Weight CMC at 1 Hz

3.3.4. Coating Elasticity

To determine the time dependence of the coating elasticity, the samples were pre-sheared at 300 s^{-1} for 10 seconds to disrupt the suspension network. Nisogi, *et al.* (2), determined that, at frequencies higher than 1 Hz, the stability of the data was very low; therefore, all time dependence experiments were performed at 1 Hz for a duration of 200 seconds acquiring data points every 5 seconds at 1% strain. After those conditions, the phase angle and storage modulus seem to reach a stable level.

The decrease in phase angle is measured as a function of time after the aforementioned shear history. This test should characterize how rapidly the particles and polymers reform into a structure after being broken down by the

shear. A fluid possessing a phase angle close to 90 degrees shows no elastic properties. This curve is expected for samples containing no polymers.

The slopes of these lines follow the logarithmic fit of

$$\delta = a\ln(t) + b \tag{3.1}$$

where δ is the phase angle, a is the slope of the line, t is time, and b is the y-intercept of the line.

The increase in their storage modulus is also measured as a function of time. The increase is G' is a better parameter to observe how rapidly the particles and polymers reform into a structure after being broken down by the shear. The curve expected for samples containing no polymer possesses a storage modulus close to zero indicating no elastic properties.

The slopes of these lines follow the logarithmic fit of

$$G' = a\ln(t) + b \tag{3.2}$$

where G' is the storage modulus, a is the slope of the line, t is time, and b is the y-intercept of the line.

3.4. Coating Methods

For this study, a laboratory rod draw down coater, a cylindrical laboratory coater, and an air-assisted spray coater were used.

3.4.1. Rod Draw Down Coater

The rod draw down coater is a laboratory scale coater used to simulate the wire-wound rods (Mayer rods) that are widely used in industry. The patterned rods are used for metering the coating and applying and distributing the suspension along the continuous web of paper. They apply a smooth coating film by the volume of coating that is between the wire (Figure 3.4) controlling the coat weight by wire diameter which is advantageous over using smooth rods that control coat weight by gap size (54).

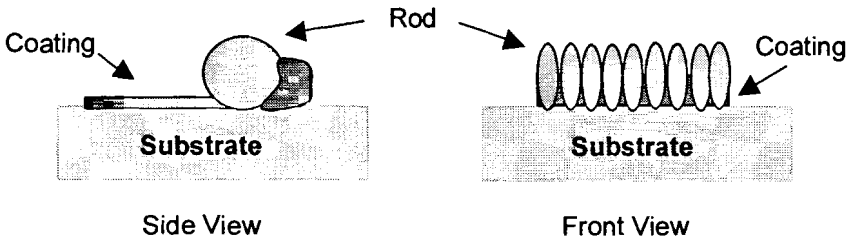

Figure 3.4 Rod Draw Down Coater

The coater used has a variable speed motor that moves the rod along the substrate at a steady speed controlling the amount of shear applied to the coating suspension. The rod is held in place by a locking mechanism and the gap is adjusted by micrometers located on either end of the rod. The gap was adjusted for each coating suspension and substrate used so that the rod was in contact with the substrate as depicted by Figure 3.4.

3.4.2. Cylindrical Laboratory Coater

Blade coating can control coat weight by changing the blade pressure, the speed of the machine, or the viscosity of the coating, resulting in high shear rates. The cylindrical laboratory coater, CLC-6000™, uses a blade to simulate industrial blade coating. The CLC was developed to help predict production problems encountered when coating formulations were taken from the laboratory testing stage to the production stage (55). The CLC can coat at speeds as high as 6000 feet per minute and utilizes programmable IR drying before and after the substrate is coated. Once the zero position of the blade against the roll is determined, the blade is manually adjusted to a gap size to obtain the desired coat weight. Figure 3.5 is a schematic of the CLC coating process. The coating suspension is contained in the stationery pond that the blade is attached to. The coater begins the coating process once the roll is rotating at the operator set speed. When coating, the pond is positioned against the web, and the pond shutter opens allowing the coating to come in contact with the web that is rotating in the counterclockwise direction.

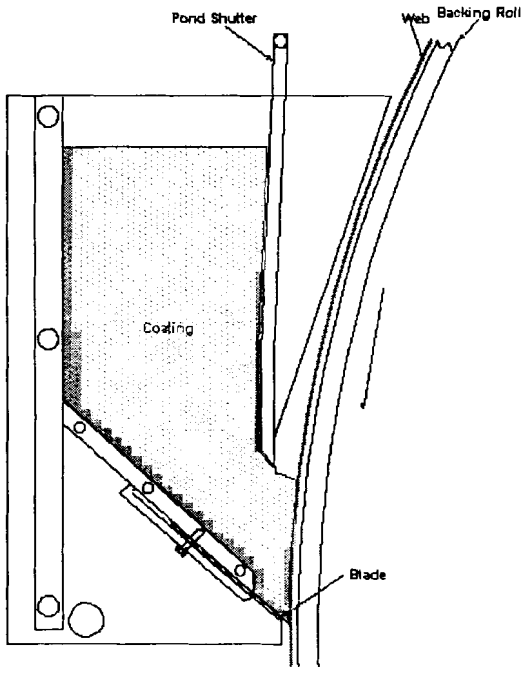

Figure 3.5 Cylindrical Laboratory Coater (CLC)

To use the CLC, paper is wrapped and taped around the backing roll, and for all experiments preformed on the CLC, the roll rotated at a speed of 3000 feet per minute. The drying time before the coating was 80% power for 10 seconds, and after coating, 25% power was used for 35 seconds. More than 25% power after coating caused visible deformities in the coating. When plastic film was used as the substrate, paper was used as a backing material on the roll, and the film was taped to the paper.

3.4.3. Air Assisted Spray Coater

The spray coater used for this study was the Binks Model 95 (Signature Series). This particular spray gun utilizes an outside high-pressure air source to pressurize the sample cup that contains the coating suspension. The

advantages of using this system are that it provides good atomization, or even drop size distribution, and has the ability to atomize highly viscous materials. It also has large passages to help prevent clogging, but the suspension can back up in the air line. Figure 3.6 shows that the liquid and air travel through different passages. They mix in the chamber just before exiting through the orifice.

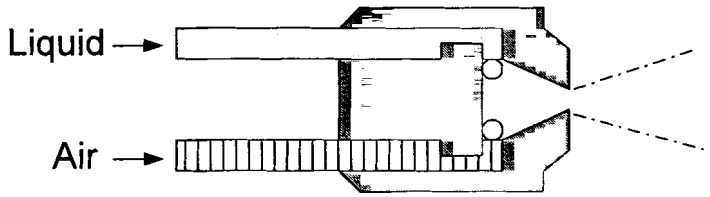

Figure 3.6 Internal-Mixing Air Assisted Spray Coater Nozzle (53)

When the spray gun was used, the cup was pressurized at 30 psi. The air flow and liquid output were adjusted for high atomization that resulted in small droplets. This adjustment resulted in high substrate coverage with low coat weights. Low atomization resulted in large droplets, poor substrate coverage, and high coat weights. The substrates were placed horizontally, and the spray gun was held about 12 inches away and was manually moved along the substrate at a relatively steady speed to ensure even coat weights.

3.5. Coating Characterization

After determining the rheological characteristics of the coating suspensions, the coatings were applied to 80 g/m^2 wood-free paper (provided by Hansol Paper) and to non-porous plastic film (AIN Plastics). The coat weight was on the order of 25 $\pm$ 5 g/m^2. Once the coatings were applied, the void

fraction, absorption, gloss, and light scattering coefficient were measured to characterize the final coating structure.

3.5.1. Void Fraction

As a means of determining the porosity of the coatings, void fraction was measured using an oil absorption technique (20) in which silicon oil was applied to a known weight of sample of area 30 cm^2. To saturate the sample, 0.5 mL of oil were applied carefully using a micropipette. The sample was allowed to become saturated for about 10 minutes, until the coating layer becomes translucent, before the excess oil was carefully removed. The sample was weighed again to determine the volume of the oil that was absorbed into the pores. The void fraction, ε, was then determined to be the ratio of volume of the air, V_a, (determined from the weight of the absorbed oil and its density) to the total volume of the coating layer, V_C (3.3).

$$\varepsilon = \frac{V_a}{V_a + V_C} \tag{3.3}$$

where

$$V_a = \frac{W_{oil}}{\rho_{oil} \cdot A} \tag{3.4}$$

and

$$V_C = \frac{f_p \cdot W_C}{\rho_p} + \frac{f_L \cdot W_C}{\rho_L} + \frac{f_{pol} \cdot W_C}{\rho_{pol}} \tag{3.5}$$

where W_{oil} represents the weight of the oil, ρ_{oil} is the density of the silicon oil, and A is the area of the sample. The subscripts, p, L, and pol represent the pigment, latex and polymer, respectively. The weight fraction of the component in the coating is represented by f, W_C represents the coat weight per unit area, and ρ is the density of the component.

For samples tested on paper, the equation (3.3) was modified as:

$$\varepsilon = \frac{V_a - V_p}{V_a + V_C - V_p} \tag{3.6}$$

where V_p is the volume of the oil absorbed by the base sheet of paper. V_p is calculated in the same manner as in Eq. (3.4). V_a is now the volume of air ing the coating and the paper. Therefore, by subtracting V_p, the void volume of the paper is corrected. This calculation is based on the assumption that there is no coating penetration into the pores of the paper and that the paper pore structure is not changed by the wetting and drying action.

The volume of the coating layer is based on the coating composition and the densities of the components. The densities of the materials used along with that of silicon oil can be found below in Table 3.3. These values were obtained from the material safety data sheets provided from the suppliers.

Table 3.3 Densities of Coating Materials

Material	Density, g/cm^3
Silicon Oil	0.963
Covergloss, Kaolin Clay	2.61
KCS, Kaolin Clay	2.62
Plastic Pigment 755 ANA BK	1.03
Plastic Pigment 723 ANA	1.03
Fine Precipitated Calcium Carbonate	2.71
Styrene Butadiene Latex	0.99
CMC	1.59
HASE, RM-232	1.02
HEUR, RM-12W	1.04

3.5.2. Absorption

Absorption rate is determined by the Bristow Absorption Test (56). The Bristow wheel is intended to measure absorption of a liquid over short time periods. The absorption of paper is important to determine the behavior of the paper for printing purposes, which relates to pore structure of coatings. A schematic is illustrated in Figure 3.7.

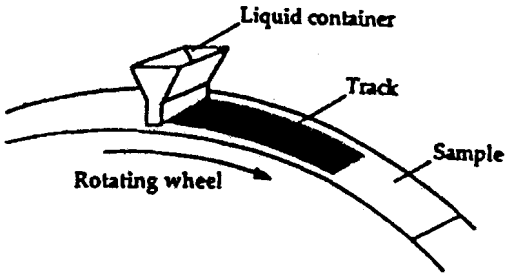

Figure 3.7 Bristow Absorption Tester (56)

The test is carried out by attaching a strip of paper to a rotating wheel. The test liquid is transferred to the liquid container using a micropipette, and when the wheel begins to rotate, the liquid is transferred to the strip of paper making a "track", which is then used to determine the area of absorption.

For this study, water containing a dye-based ink was used at a volume of 10 μL, and the wheel rotated at a rate of 0.2 cm/s. The total liquid volume (T. L. V.) transferred to the paper sample is the ratio of the volume of water to the area of absorption (3.7).

$$TLV = \frac{L * V}{A} \tag{3.7}$$

where L is the track length, V is the volume of the liquid (10 μL), and A is the area of the track length.

The area of the track length is found by multiplying the trace length by the length of the slot of the liquid container (1.5 cm). The contact time is calculated from the ratio of the width of the slot of the liquid container (0.1 cm) to the speed

of rotation (0.2 cm/s). For all absorption experiments, the contact time was 0.5 seconds.

3.5.3. Gloss

The gloss is a relative measure of the surface smoothness and is important in the printability of coated papers. Gloss is important in this investigation to confirm the existence of a structure network. If a bulkier structure exists, then the surface may be rough resulting in a lower gloss measurement.

Gloss is measured by reflecting light onto the coated sample. The light is directed through a series of lens that create in parallel beams. The light is scattered upon hitting the sample and is detected by a photo-detector after traveling through lens and filters, which eliminates all excess light and detects only the parallel beams. For this study, gloss was obtained using a HunterLab Modular Glossmeter, Model D48-7, a standard TAPPI 75° incident light angle glossmeter that was standardized using a tile of gloss 54.0 since this was an average gloss value of the coated papers in this study. A schematic of this meter is illustrated in Figure 3.8.

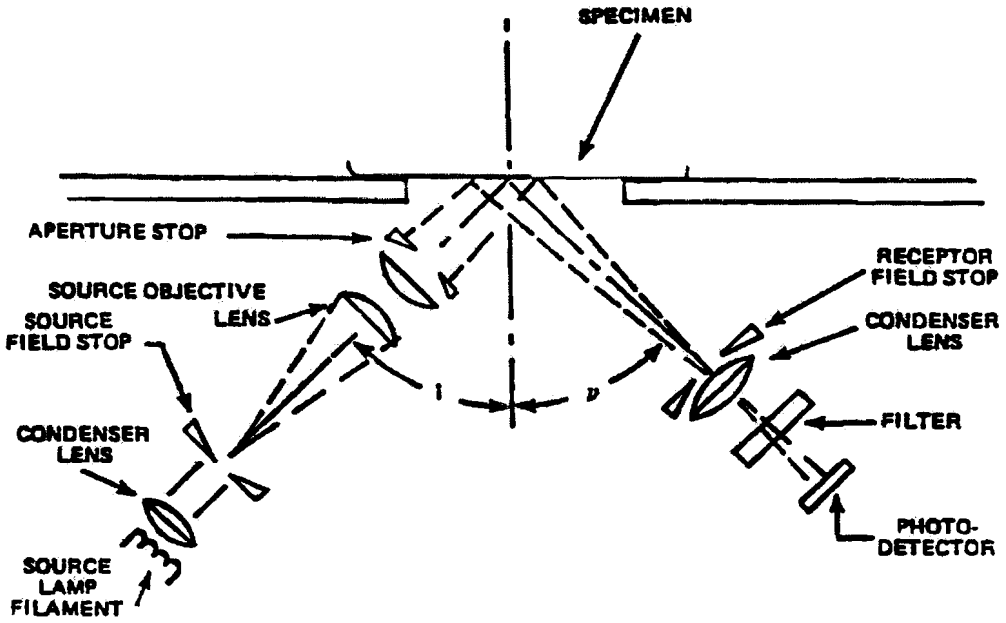

Figure 3.8 Optical System of HunterLab Modular Glossmeter, Model D48-7 (57) Where *i* is the Angle of Incident and *v* is the Angle of Reflectance

3.5.4. Light Scattering Coefficient

The apparatus used for this measurement is the Technibrite Micro TB-1C made by Technidyne Corporation. The samples were tested using the "QC" mode which enables the user to take an average of several measurements from the paper sample (five measurements were averaged for each sample). This mode also measures reflectance of the paper against a black cavity and the reflectance against a thick pad of paper. For all of the experiments on paper and plastic film, about six sheets of 80 g/m^2 basis paper were used as the pad of paper.

The diffuse geometry, as seen in Figure 3.10, is utilized by this instrument. The circle (position 1) represents the sphere, 6 inches in diameter that is coated with barium sulphate paint for high reflectance. The sample is placed on a spring

loaded sample holder at position 2, which has an opening of 34 mm at the bottom of the sphere. Two halogen lamps (position 6) provide the light that is projected through lenses (position 5) and filtered by infrared heat absorbing filters (positions 3 and 4). This light is reflected off the lining of the sphere onto the sample. Position 7 is a black gloss trap to absorb specularly reflected light from the sample. An objective lens (position 8) focuses the light through a filter (position 10) and through the aperture of diameter 30 mm. The light then is reflected on the photocell before being processed. From the side view of Figure 2.10, positions 9, 11, 13, and 15 are the same system as just described, but its purpose if to detect the light being reflected off the sphere instead of the sample. The instrument was calibrated by calibrating the brightness using a built-in standard.

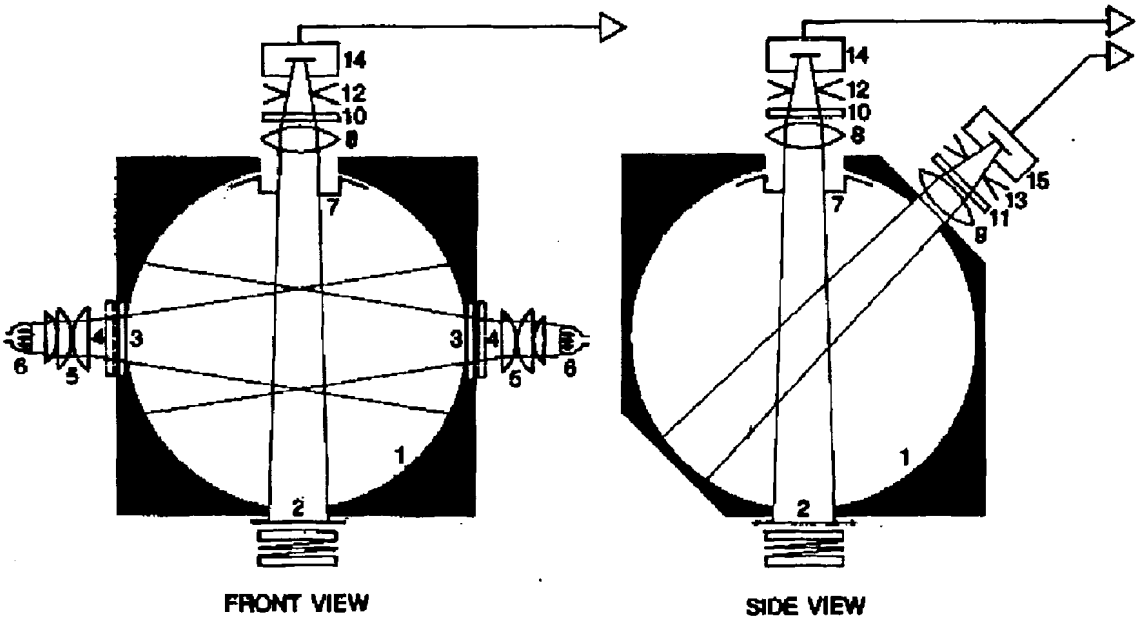

Figure 3.9 Optical System of the Technibrite Micro TB-1C (58)

The instrument used measures the brightness and the opacity of the sheet. These measurements are based on reflectance, R, which has two factors: (1) the *intrinsic reflectance factor* (R_∞) that is reflectance measured from a stack of sheets thick enough to be opaque (Figure 3.11, b.); and (2) the *black cavity reflectance factor* (R_0) that is the reflectance measured when a single sheet is placed over a black cavity (Figure 3.11, c.). Figure 3.11a. shows the reflectance of light, i_0, as it hits the paper, some of the light is scattered by the paper, some is absorbed by the paper, some is transmitted through the paper, i_T, and the rest of the light is reflected off the paper, i_{Ref}.

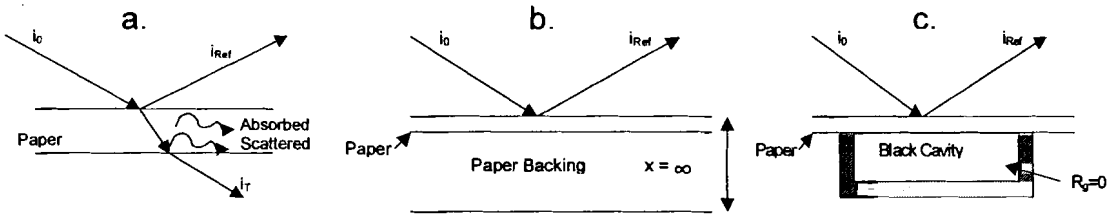

Figure 3.10 Reflectance of Light

The specific scattering coefficient (cm^2/g), S, is calculated as

$$S = \frac{s}{\rho} \tag{3.8}$$

where s is the scatter coefficient (cm^{-1}), and ρ is the density (g/cm^3).

The specific absorption coefficient (cm^2/g), K, is calculated as

$$K = \frac{k}{\rho} \tag{3.9}$$

where k is the absorption coefficient (cm^{-1}), and ρ is the density (g/cm^3).

The *brightness* is the intrinsic reflectance, R_∞, of the blue light at the effective wavelength of 457 nm since the blue area of the spectrum changes most during the paper making process (58). Brightness is determined by

$$R_\infty = 1 + \frac{K}{S} + \sqrt{\left(\frac{K}{S}\right)^2 + 2\left(\frac{K}{S}\right)} \tag{3.10}$$

The *opacity* (C) is the measure the ability of the paper to hide any material placed behind it and is determined by the black cavity reflectance factor divided by the intrinsic reflectance factor (3.9).

$$C = \frac{R_0}{R_\infty} \tag{3.11}$$

where

$$R_0 = \frac{\exp\left[sW\left(\frac{1}{R_\infty} - R_\infty\right)\right] - 1}{\frac{1}{R_\infty}\exp\left[sW\left(\frac{1}{R_\infty} - R_\infty\right)\right] - R_\infty} \tag{3.12}$$

where W is the infinite thickness of the paper backing.

To determine the reflectance factor, R, the solution to the Kubelka-Monks (59) equation can be written as

$$R = \frac{\left[\left(R_g - R_\infty\right)/R_\infty\right] - \left[R_\infty\left(R_g - 1/R_\infty\right)\right]\exp\left\{sW\left[\left(1/R_\infty\right) - R_\infty\right]\right\}}{\left(R_g - R_\infty\right) - \left(R_g - 1/R_\infty\right)\exp\left\{sW\left[\left(1/R_\infty\right) - R_\infty\right]\right\}} \tag{3.13}$$

where R_g in the reflectance of the backing.

When equation (3.13) is solved for the light scatter coefficient, s, the result is

$$s = \frac{1}{W\left(1/R_\infty - R_\infty\right)} \ln\left[\frac{\left(R_g - R\infty\right)\left(R - 1/R_\infty\right)}{\left(R - R_\infty\right)\left(R_g - 1/R_\infty\right)}\right] \tag{3.14}$$

where W is the basis weight (g/m^2) of the sample. If it is assumed that R_g is zero for the black cavity and let R become R_0, the black cavity reflectance, then the result is

$$s = \frac{1}{W\left(1/R_\infty - R_\infty\right)} \ln\left[\frac{1 - R_\infty R_0}{1 - R_0/R_\infty}\right] \tag{3.15}$$

Equation (3.13) is the calculation utilized by the Technibrite Micro TB-1C so that the light scattering coefficient is calculated based on the user defined basis weight (58).

For samples coated on paper, the mixing rule was utilized in this form:

$$s_{cp} = \left[\left(\frac{P}{W}\right)_{cp} - \left(\frac{W_p \cdot s_p}{W_{cp}}\right)\right]\frac{W_{cp}}{W_c} \tag{3.16}$$

where s_{cp} is the light scatter coefficient of the coated paper (cp), P is the measured scatter power that is used to calculate the scatter coefficient, W_{cp} is the total basis weight of the coated paper (coat weight plus paper basis weight) and W_p is the basis weight of the paper, s_p is the scatter coefficient of the basis paper, and W_c is the coat weight of the coated paper sample.

4. EFFECT OF CARBOXYMETHYL CELLULOSE

To gain a better understanding on the role of polymer molecular weight and concentration on rheology and structure, a series of CMC molecular weights and concentrations are compared. Molecular weights of 120,000; 350,000; and 700,000 daltons were compared at a concentration of 0.1 pph. Refer to Table 3.1 for the coating formulations.

Concentrations of 0.1, 0.3, 0.5, and 0.8 pph CMC were compared to understand the effect of polymer concentration on the system. Table 3.2 reports the coating formulations. Different pigments were compared using low molecular weight CMC to study the effect of the pigment on the system. For coating formulations, refer to Table 3.2.

4.1. Rheological Experiments

The suspensions were characterized for their steady shear viscosity. Figure 4.1 is a plot of viscosity as a function of shear rate for this study. All formulations contain 0.1 pph CMC and 60% solids by weight. Figure 4.1 illustrates that, as the molecular weight of the CMC increases, the viscosity increases over the range of shear rates. The sample containing no CMC has a smaller slope than the samples containing CMC which indicates that the clay and latex suspension behaves almost Newtonian. The sample containing low molecular weight CMC has a slightly lower viscosity than the sample containing no CMC. At low molecular weight, the CMC creates a smaller double layer than the higher molecular weight samples, acting as a lubricant to allow the pigment

particles to move with less friction than the sample containing no CMC (60). As the molecular weight increases, the double layer increases resulting in higher viscosities as seen in Figure 4.1.

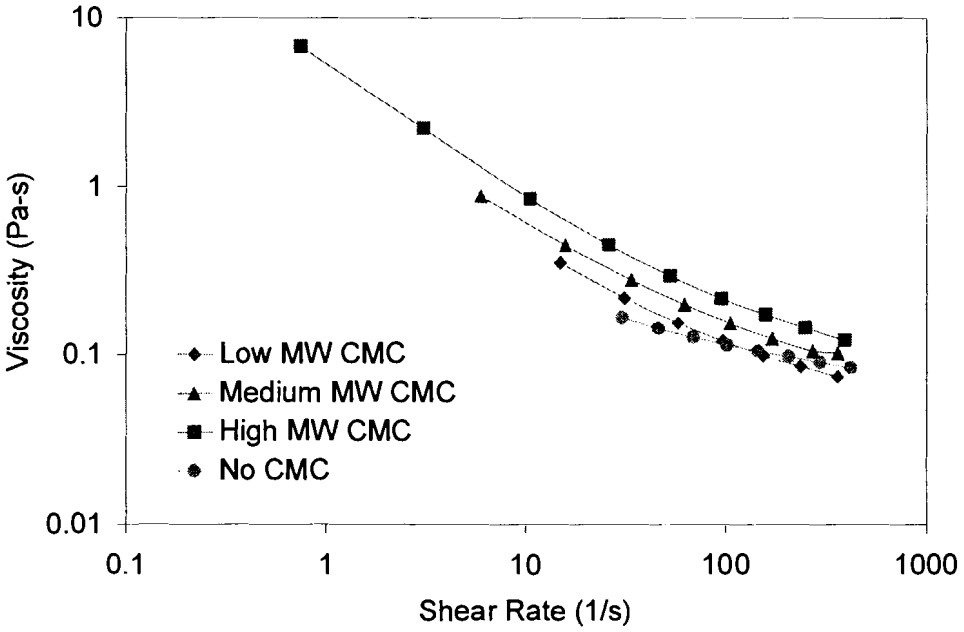

Figure 4.1 Steady Shear Viscosity for CMC Molecular Weight Comparison (0.1 pph CMC, 60% solids)

Figure 4.2 shows the oscillatory data as a function of frequency for these three coatings. As can be seen from this data, the storage modulus, G', and the loss modulus, G", show no correlation with the changing molecular weight of CMC. Note that the G' is dominant over the range of frequency shown in Figure 4.2 and it is relatively constant. With no CMC present in the system, the suspension behaves like a viscous liquid with little elastic properties.

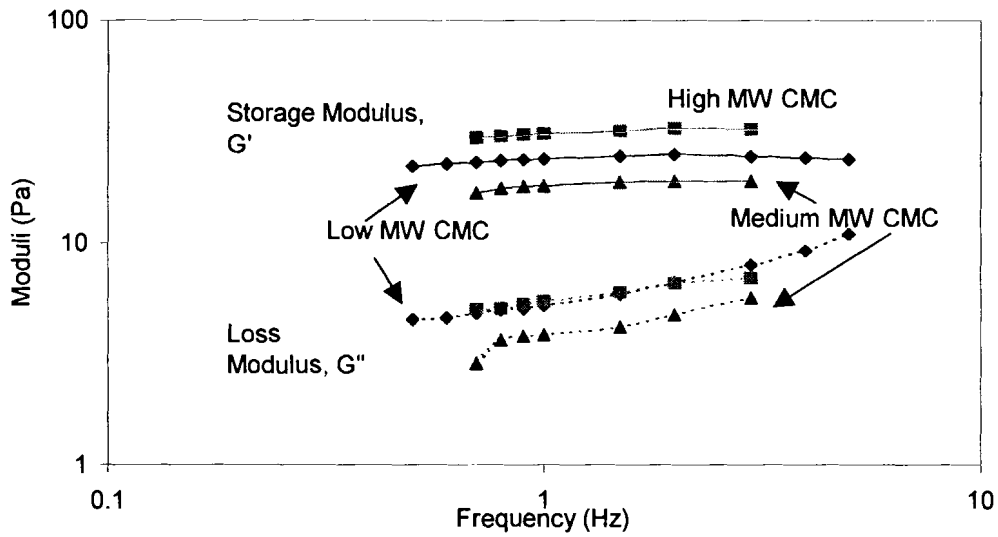

Figure 4.2 Oscillatory Measurement for CMC Molecular Weight Comparison, for the Same Coatings as Figure 4.1

Figure 4.3 shows that after shear, the phase angle decreases with time. This indicates that some elastic structure develops in the coating after shear. When CMC is present, elasticity is significant. Changing the molecular weight of the CMC has no significant affect on the slope of these lines.

The slopes of these lines follow the logarithmic fit of equation (3.1). Table 4.1 shows the values of this fit for these additives. The slope of the sample with no CMC does not fit equation (3.1), but all other samples fit reasonably well. When considering the slopes of the lines of the suspensions with CMC, there is little change in rate of structure reformation as a function of the molecular weight of CMC. Structure reformation is expected to be a diffusional process with pigments and polymers finding a low energy state due to diffusion. When the

slope is normalized by the final phase angle, this value increases slightly as the molecular weight increases indicating slower diffusion of particles.

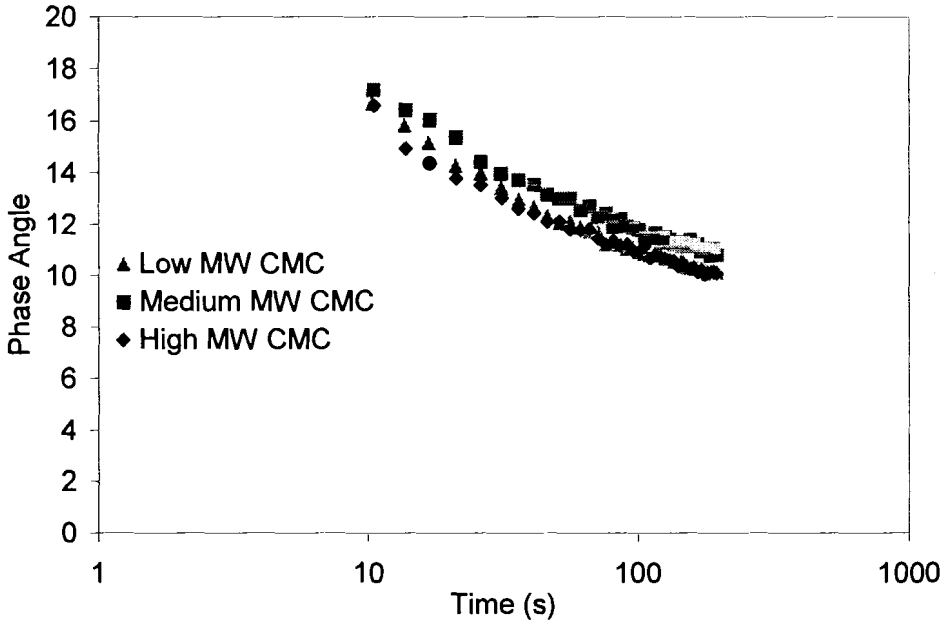

Figure 4.3 Phase Angle for CMC Molecular Weight Comparison, for the Same Coatings as Figure 4.1

Table 4.1 Logarithmic Fit of Phase Angle and Time Relationship for Varying CMC Molecular Weights

Phase Angle, δ	δ_{Final}	a	a/δ_{Final}	b	R^2
No CMC	69.94	-2.91	-0.0416	90.46	0.0232
Low MW CMC	10.23	-2.06	-0.201	20.65	0.9686
Medium MW CMC	11.05	-2.05	-0.186	21.34	0.9706
High MW CMC	10.18	-1.87	-0.184	19.69	0.9629

Figure 4.4 shows the change in storage modulus after shear. The suspension containing no CMC confirms the phase angle data that the suspension behaves much like a viscous liquid without elastic properties. Table 4.2 contains the fit parameters of equation (3.1). The sample with the medium molecular weight has the lowest slope. When looking at the rate of structure recovery in terms of G', no correlation is obvious with the molecular weight. However, the phase angle does follow a pattern. When the slope is normalized by the final G', a trend is observed that agrees with the pattern of the phase angle, as the molecular weight increases, the a/G' value decreases.

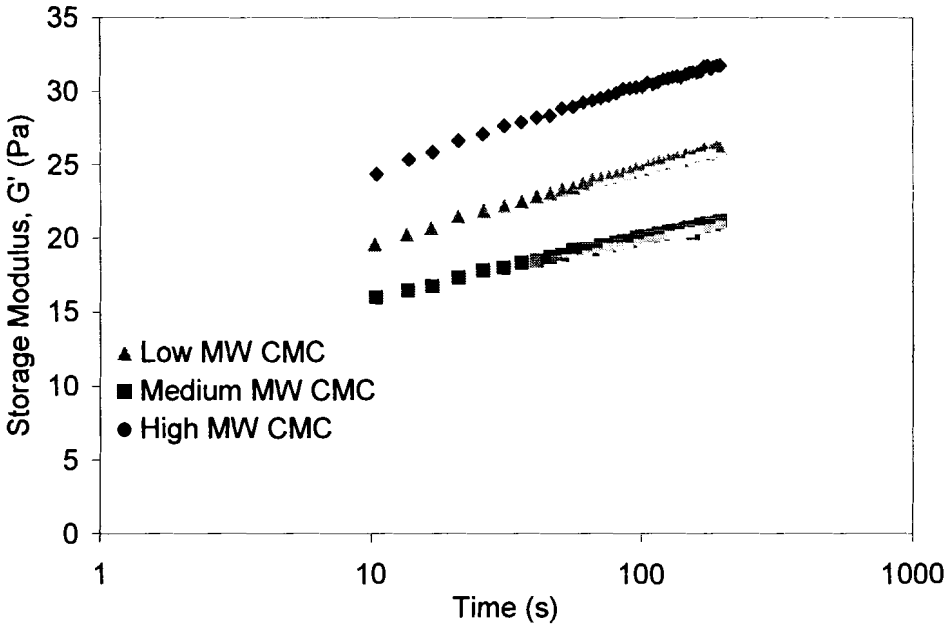

Figure 4.4 Storage Modulus for CMC Molecular Weight Comparison, for the Same Coatings as Figure 4.1

Table 4.2 Logarithmic Fit of Storage Modulus and Time for Varying CMC Molecular Weights

Storage Modulus, G'	G'_{Final}	a	a/G'_{Final}	b	R^2
No CMC	1.74	0.56	0.320	-0.606	0.0836
Low MW CMC	25.87	2.18	0.0843	14.69	0.9970
Medium MW CMC	20.86	1.70	0.0815	12.14	0.9941
High MW CMC	31.53	2.42	0.0768	19.13	0.9954

4.2. Coating Characteristics as a Function of CMC Molecular Weight

In Figure 4.5, void fraction is plotted as a function of molecular weight. The coat weight for these samples on plastic film and paper was 32 ± 2 g/m^2. The coefficient of variance of the void fraction is about 4% for 6 samples tested on plastic film and 3% to 18% for six samples tested on paper. Even though the storage modulus increased with CMC molecular weight, the void fraction had little change. This result is different from Nisogi *et al.* (1), where void fraction increased with increasing storage modulus.

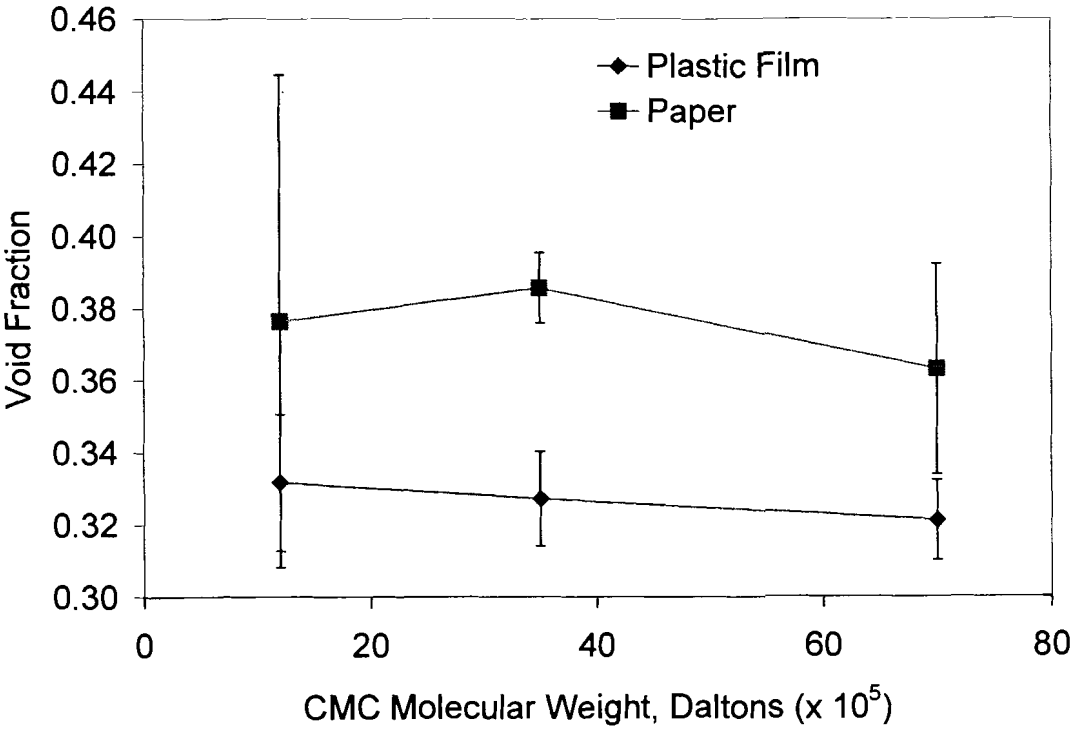

Figure 4.5 Void Fraction as a Function of CMC Molecular Weight for 0.1 pph

Figure 4.6 shows the volume of water absorbed at 0.5 seconds contact time as a function of CMC molecular weight. Changing the molecular weight of the CMC has no significant effect on the water absorption on paper or plastic film. The results of the absorption test confirm the void fraction results. The coefficient of variance on paper is less that 3% and on plastic film is less that 7% for six samples tested.

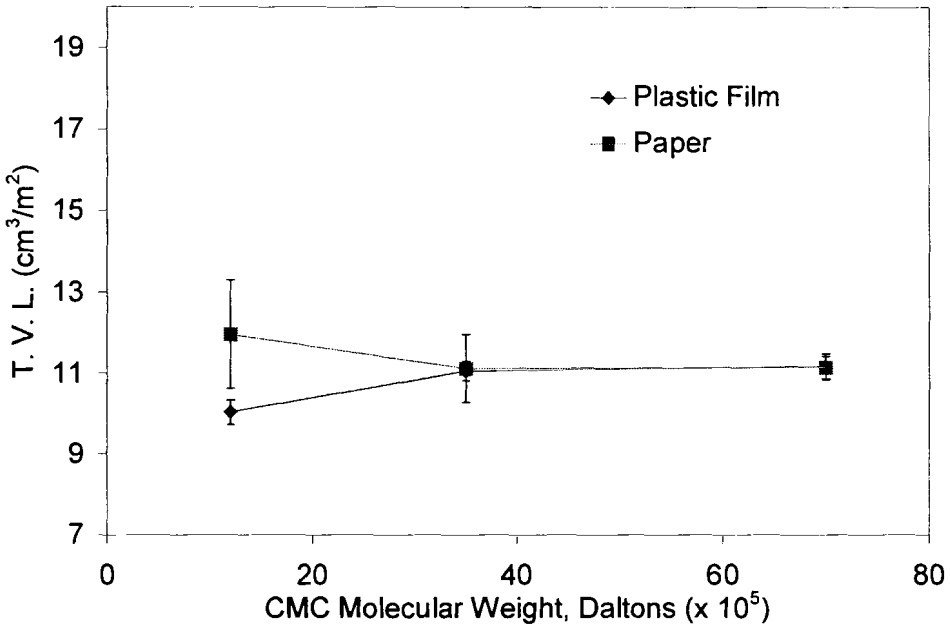

Figure 4.6 Water Absorption as a Function of CMC Molecular Weight for the Coatings in Figure 4.5

Figure 4.7 shows that an increase the molecular weight results in a decrease in coating gloss. This result indicates that the high molecular weight system may reduce the leveling rate of the rod marks causing a rougher surface than the low molecular weight system. The leveling rates of small defects should scale with low shear rate viscosity. The high molecular weight CMC had the largest viscosity at low shear rates.

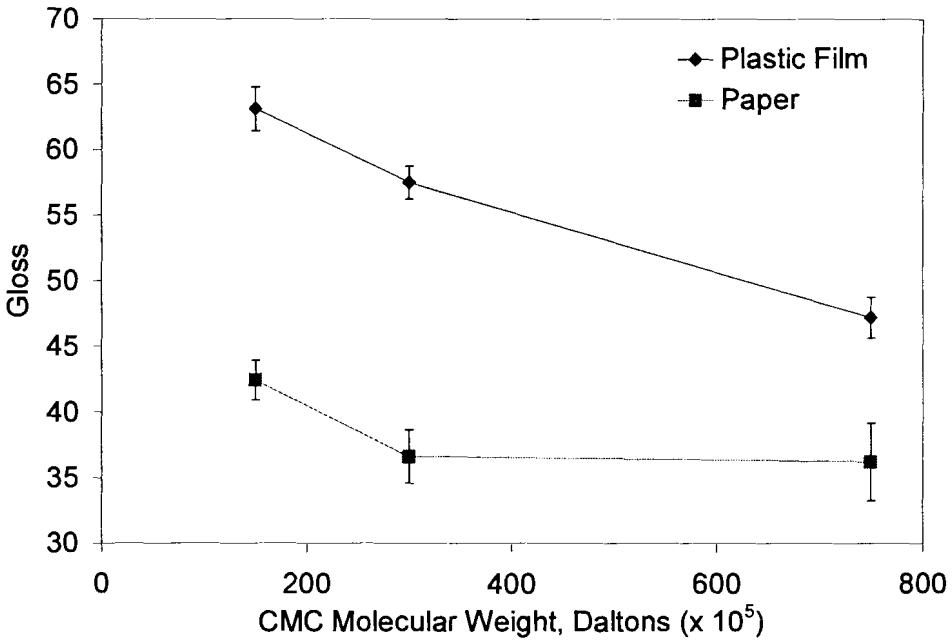

Figure 4.7 Gloss as a Function of CMC Molecular Weight for the Coatings in Figure 4.5

Figure 4.8 reports the LSC on plastic film and paper. On plastic film, the LSC seems to decrease slightly, but the change is not significant. On paper, there is no significant change as the molecular weight of CMC increases. The void fraction and water absorption results agree with the light scattering coefficient.

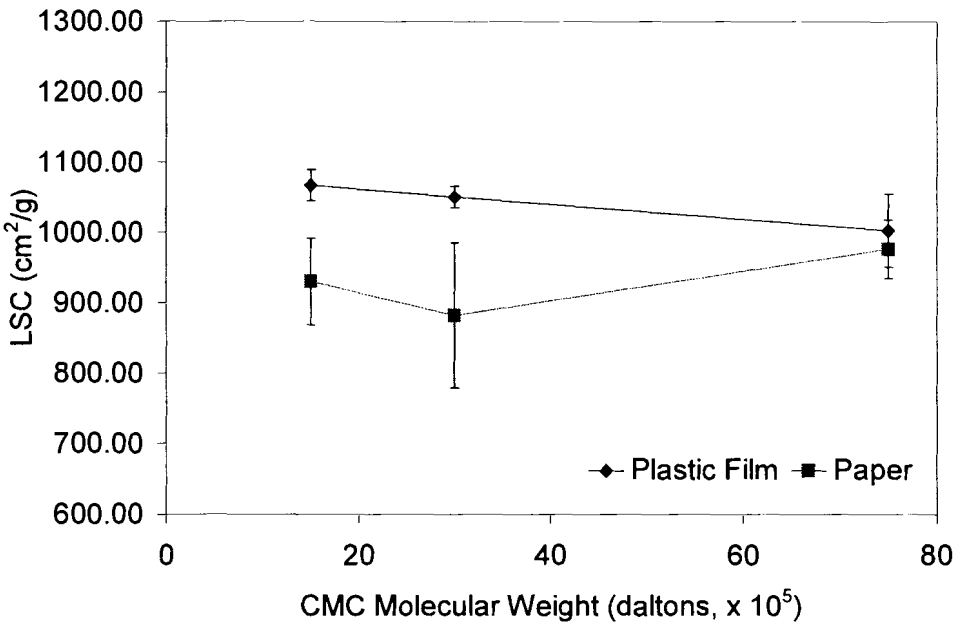

Figure 4.8 Light Scattering Coefficient as a Function of CMC Molecular Weight for the Coatings in Figure 4.5

4.3. Influence of CMC Concentration

Nisogi *et al.* (1) found that increasing the polymer concentration resulted in increasing storage modulus, void fraction and LSC. To compare with these findings, the concentration of CMC is varied.

As with the varying molecular weight experiments, the suspensions were characterized for their steady shear viscosity. Figure 4.9 shows viscosity as a function of shear rate. As the concentration of CMC increases, the viscosity of the suspension increases over the range of shear rates studied. As with the previous discussion in Section 4.1, the 0.1 pph sample has a lower viscosity than the sample containing no CMC. At low concentration, the CMC has less surface

coverage than the higher concentration samples, acting as a lubricant to allow the pigment particles to move with less friction than the sample containing no CMC (60). The viscosity of the 0.5 pph sample and the 0.8 pph sample has identical curves. A maximum influence on rheology with concentration may be reached at this point.

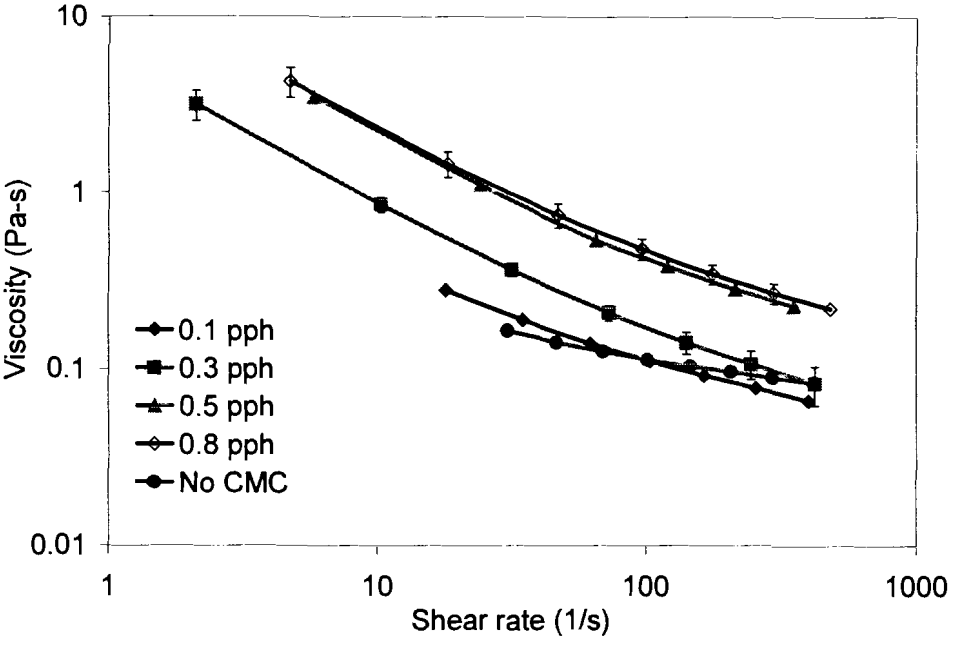

Figure 4.9 Steady Shear Viscosity for Varying CMC Concentrations

Figure 4.10 shows the oscillatory data as a function of frequency for these coatings. As seen from this data, G' and G" increase with increasing additive concentration. All of the curves are the same, just shifted up as the CMC concentration increases. G' also remains dominant over the range of frequency from 0.5 Hz to 5 Hz. As with the varying molecular weight experiments, G' and

G" remain relatively constant over this frequency range. Again, the 0.5 pph sample and the 0.8 pph sample seem to have similar curves.

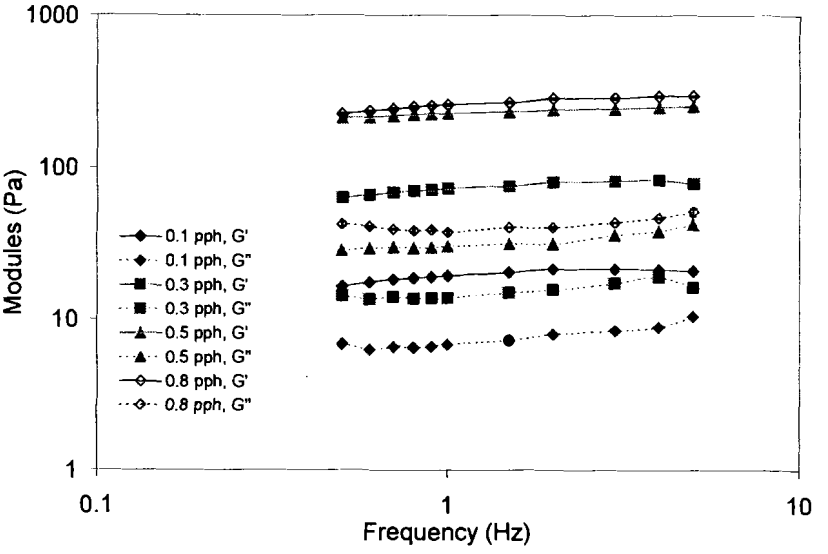

Figure 4.10 Oscillatory Measurements for Varying CMC Concentrations, for the Coatings in Figure 4.9

Figure 4.11 illustrates the change in phase angle as a function of time after a steady shear. This data shows that as polymer concentration increases, the phase angle decreases as a function of time. This behavior is similar to the findings of Nisogi *et al.* (2) for the HASE system. The slopes of these lines follow the logarithmic fit of equation (3.1). Table 4.3 shows the values of this fit for these additives. The slope of the sample with no CMC does not fit equation (3.1), but all other samples fit well. As mentioned before, the final phase angle decreases with increasing additive concentration. The slopes of the lines seem to become less steep from 0.1 to 0.5 pph. This may indicate an increased difficulty in diffusion to rebuild the structure. As with the other rheological tests,

0.5 and 0.8 pph concentrations behave the same. When the slope of these lines are normalized with the final phase angle, this value decreases with increasing CMC concentration, and a difference between the 0.5 and 0.8 pph concentrations is observed. This is explained by the particles moving more rapidly in a diffusional process.

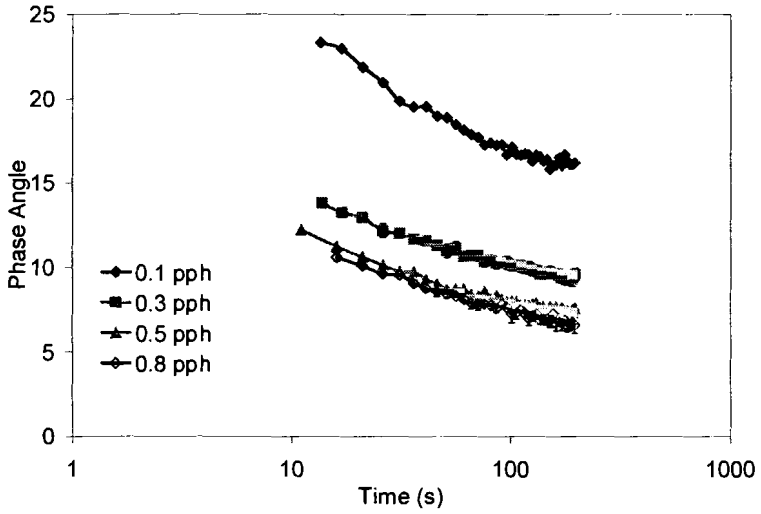

Figure 4.11 Phase Angle After Steady Shear for Varying CMC Concentrations, for the Coatings in Figure 4.9

Table 4.3 Logarithmic Fit of Phase Angle and Time Relationship for Varying CMC Concentrations

Phase Angle, δ	δ_{Final}	a	a/δ_{Final}	b	R^2
No CMC	69.94	-2.91	-0.0416	90.46	0.0232
0.1 pph CMC	16.25	-2.62	-0.161	29.34	0.9448
0.3 pph CMC	9.13	-1.57	-0.172	17.48	0.9751
0.5 pph CMC	7.51	-1.51	-0.201	15.11	0.9524
0.8 pph CMC	6.93	-1.54	-0.222	14.64	0.9769

Figure 4.12 represents the change in storage modulus as a function of time for these coatings. There is a systematic increase in the modulus and its slope. Table 4.4 shows the slope and intercept for the logarithmic fit for these additives. The slope of the sample with no additive does not fit Equation (3.1), but all other samples fit well. The G' increases with increasing additive concentration, and the slopes of the lines also increase with increasing additive concentration. This behavior agrees with the findings of Nisogi *et al.* (2). The slopes of phase angle curves did not show a trend with concentration. Upon normalizing the slope with the final G', from 0.1 to 0.5 pph, this normalized value decreases, but the 0.8 pph sample does not fit the trend.

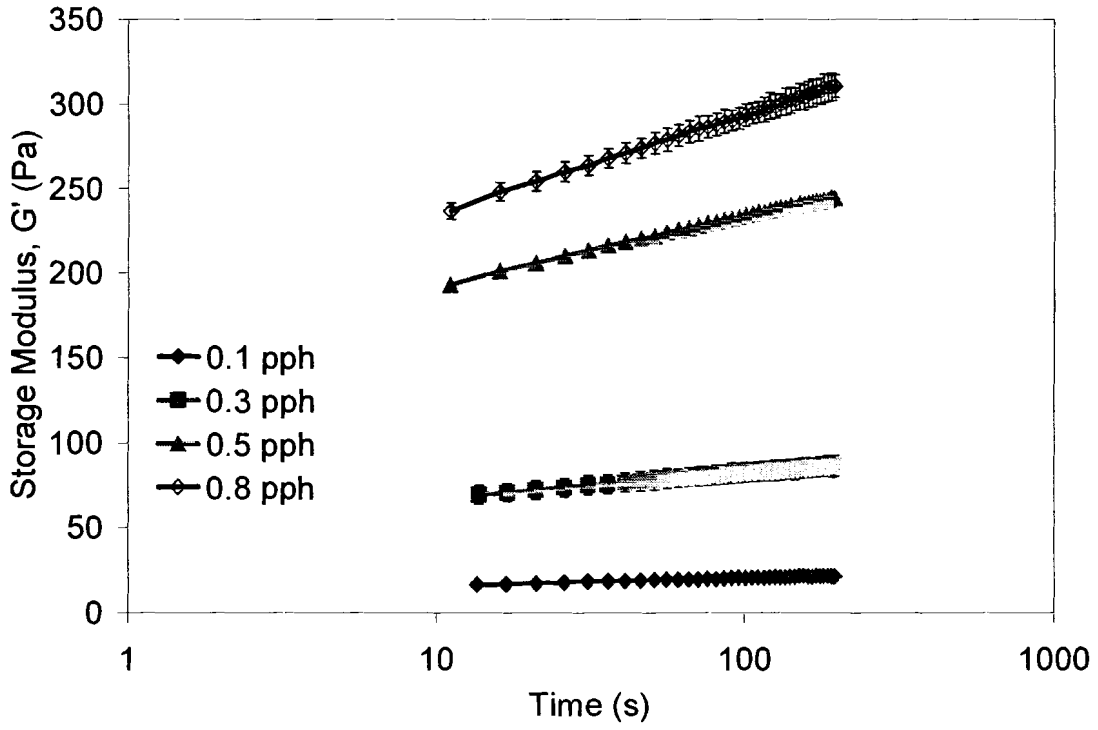

Figure 4.12 Storage Modulus for Varying CMC Concentrations, for the Coatings in Figure 4.9

Table 4.4 Logarithmic Fit of Storage Modulus and Time Relationship for Varying CMC Concentrations

Storage Modulus, G'	G'_{Final}	a	a/G'_{Final}	b	R^2
No CMC	1.74	0.56	0.320	-0.606	0.0836
0.1 pph CMC	21.57	1.92	0.0890	11.68	0.9911
0.3 pph CMC	82.72	6.38	0.0771	52.90	0.9982
0.5 pph CMC	243.35	17.49	0.0719	153.02	0.9974
0.8 pph CMC	309.11	25.28	0.0818	177.04	0.9992

4.4. Coating Characteristics as a Function of the CMC Concentration

The void fraction was considered as a function of concentration as seen in Figure 4.13. The coat weight of the samples tested on plastic film and paper was 25 ± 3 g/m^2. The 0.1 pph concentration resulted in a drop in void fraction on plastic film, but no trend was found in the void fraction, on plastic film, as the polymer concentration was increased. This behavior indicates that although CMC provides coating elasticity, it has no affect on the final coating porosity. No conclusion could be made for samples on paper due to the error in this measurement and other possible artifacts. Figure 4.13 is plotted as a function of CMC concentration, but concentration is directly correlated with the increasing storage modulus. These results are contrary to what Nisogi *et al.* (1) found for the HASE system: as the polymer concentration increases, the void fraction increases. However, these results can be compared to those found by Rousu *et*

al. (61) who used different variables and different testing methods to determine as relationship between the wet suspension and the final coating structure. They determined that CMC does affect the void fraction to an extent due to the absorption behavior of the polymer. The coefficient of variance of void fraction is less than 4% for six samples tested on plastic film and 20% on paper.

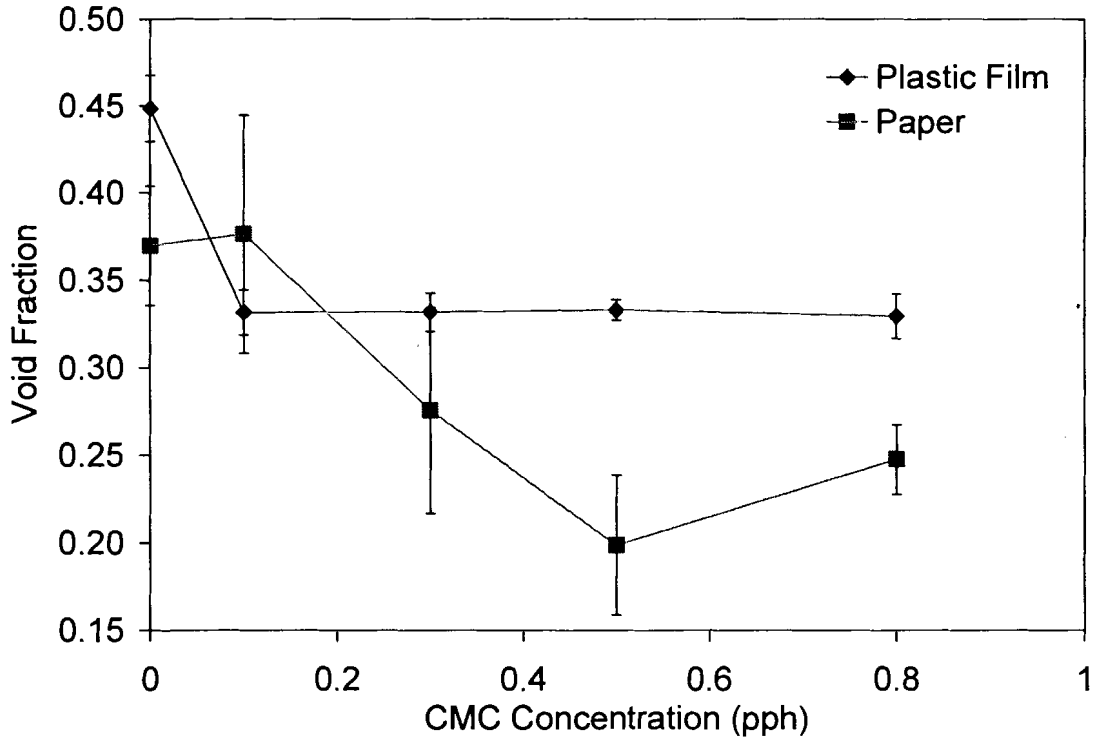

Figure 4.13 Void Fraction as a Function of CMC Concentration, for the Coatings in Figure 4.9

The absorption results are plotted as a function of CMC concentration in Figure 4.14. There is little change in the water absorption as the CMC concentration increases. These results confirm the void fraction results that there is no correlation between increasing polymer concentration and void

fraction. The coefficient of variance for the void fraction is less than 6% for six samples tested.

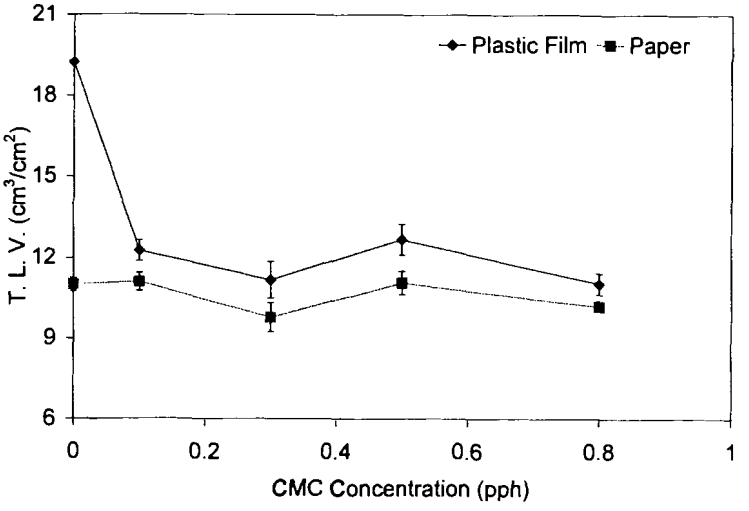

Figure 4.14 Water Absorption as a Function of CMC Concentration, for the Coatings in Figure 4.9

Figure 4.15 suggests that the gloss as a function of CMC concentration decreases as the CMC concentration increases. The leveling is slower for the higher CMC concentrations. The coefficient of variance for the gloss is less than 4% on paper and plastic film.

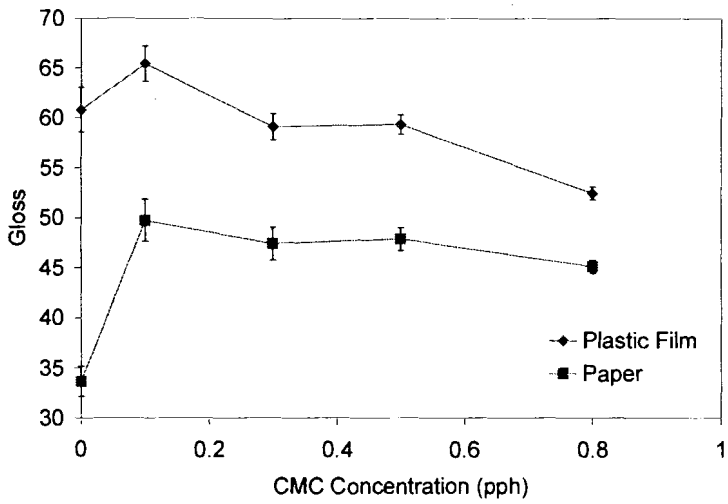

Figure 4.15 Gloss as a Function of CMC Concentration for the Coatings in Figure 4.9

The LSC is plotted as a function of CMC concentration in Figure 4.16 for samples on both paper and plastic film. There is no significant change in the LSC as a function of CMC concentration. The void fraction and water absorption data suggests that the sample containing no CMC has high voids compared to the other concentrations for samples coated on plastic film. In this case, the LSC may be a more accurate measurement of pore size since the trends on paper and plastic film are similar. This data agrees with the void fraction on paper, and the water absorption. The coefficient of variance for the LSC is about 4%.

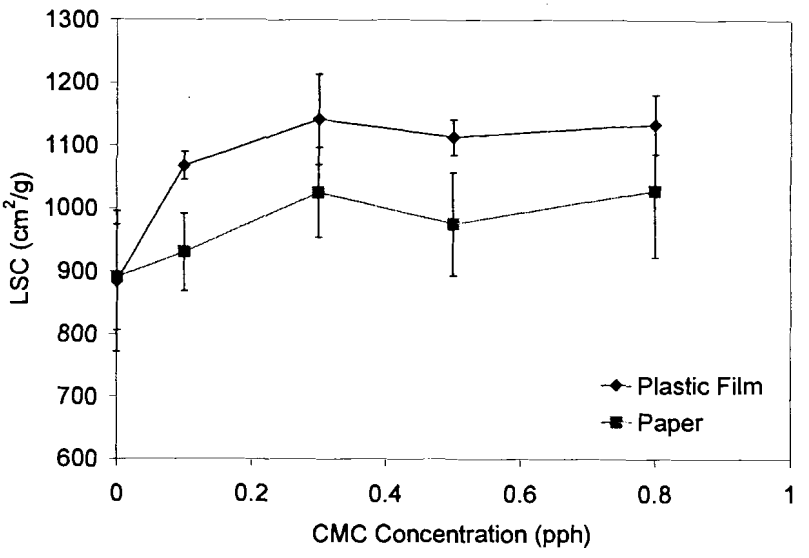

Figure 4.16 Light Scattering Coefficient as a Function of CMC Concentration for the Coatings in Figure 4.9

4.5. Influence of Pigments

The rheological data for a few other pigment systems had quite different results and could not be attained without modifying the suspension with other additives such as salt that would create a thicker double layer around the pigment particles stabilizing the suspension. After a steady shear, both plastics pigments tested did not fit the logarithmic fit as the other systems have because they had low elasticity. Figure 4.17 shows that when 0.1 pph medium molecular weight CMC was used, the storage modulus of both plastic pigments fit a fifth order polynomial as compared to the delaminated clay sample that fits equation (3.1). This behavior was also the case for the phase angle.

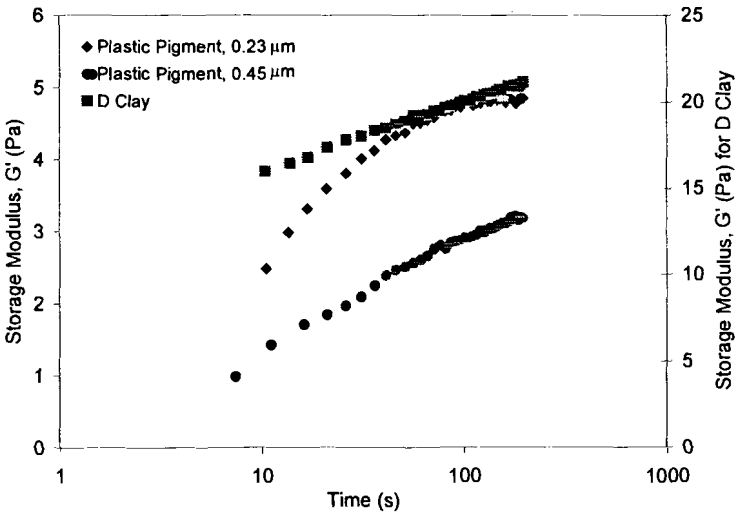

Figure 4.17 Storage Modulus for Plastic Pigments Having a Pigment Volume Concentration of 0.309 Containing 0.1 pph Medium MW CMC

Figure 4.18 shows the storage modulus for the medium precipitated calcium carbonate. A decrease in storage modulus as a function of time was observed, and an increase in phase angle was observed for this system. This behavior was caused by settling of the pigments during the rheology tests.

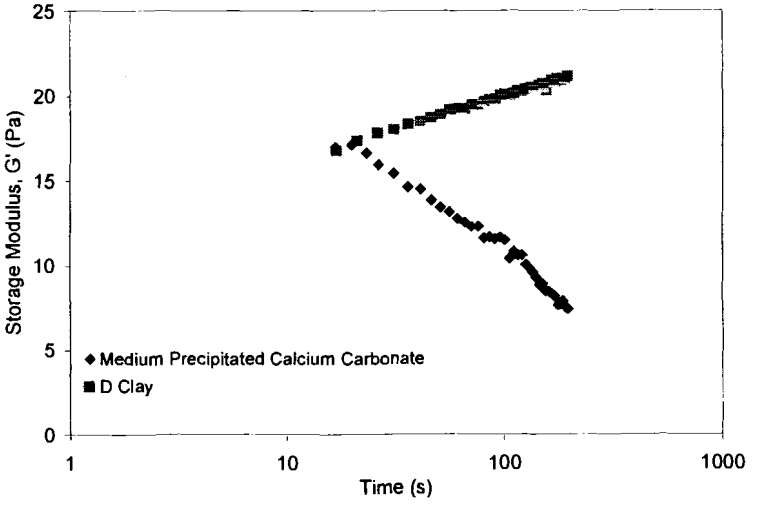

Figure 4.18 Storage Modulus for Precipitated Calcium Carbonate Having a Pigment Volume Concentration of 0.309 Containing 0.1 pph Medium MW CMC

The rate of increase in the storage modulus for three different plastic pigment sizes is much lower than the kaolin pigment indicating the rate of increase in the storage modulus depends on the pigment size. Therefore, the diffusion of pigment particles, by Brownian motion, seems to be the rate-controlling step for the increase in the storage modulus after shear. The $CaCO_3$ pigment results were attributed to the settling of the particles during the test and does not relate to the structure of the pigments.

Figure 4.19 is a depiction of the void fraction as a function of storage modulus for the different pigments tested with 0.1 pph CMC in the plastic pigment, 0.45 μm, and the medium $CaCO_3$ and 0.3 pph CMC in the plastic pigment, 0.23 μm, the #2 grade clay, and the delaminated clay. These formulations were based on the pigment volume concentration. From this data, there is no correlation between storage modulus and void fraction. These pigments were also tested for shape and particle size. The plastic pigments and the $CaCO_3$ are spherical and are plotted in order of increasing particle size. No distinct correlation is present with respect to particle size. The clays are plate like in shape, and the #2 grade clay has a broad particle size distribution where as the delaminated clay has a narrow particle size distribution. The delaminated clay has a slightly higher storage modulus but lower void fraction than the #2 grade clay. The #2 grade clay may be packing differently than the delaminated clay because of the finer and larger particles that may be present in the system.

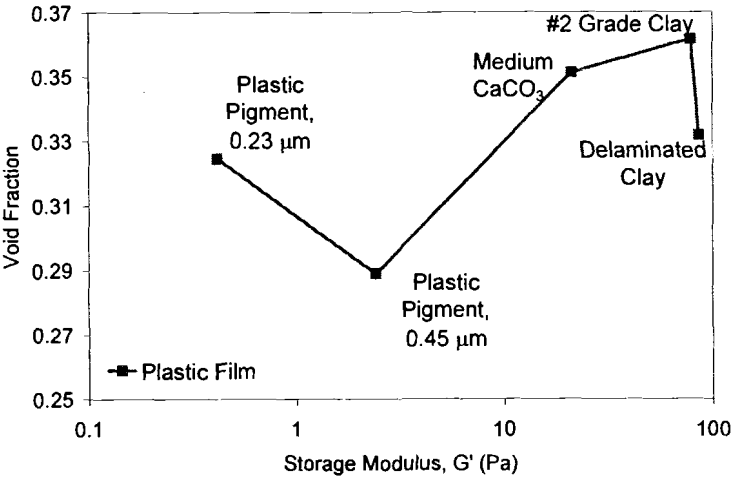

Figure 4.19 Void Fraction as a Function of Storage Modulus for Different Pigments all at Coat Weights of 25 ± 5 g/m^2 and Pigment Volume Concentrations of 0.309

Figure 4.20 represents the gloss data for the different pigments. There is no distinct correlation between storage modulus and gloss because the shape and particle size for the plastic pigments and $CaCO_3$ are more important. The clays also show no distinct correlation with particle size distribution, storage modulus, and gloss. These same trends observed for gloss confirm those observed for the void fraction.

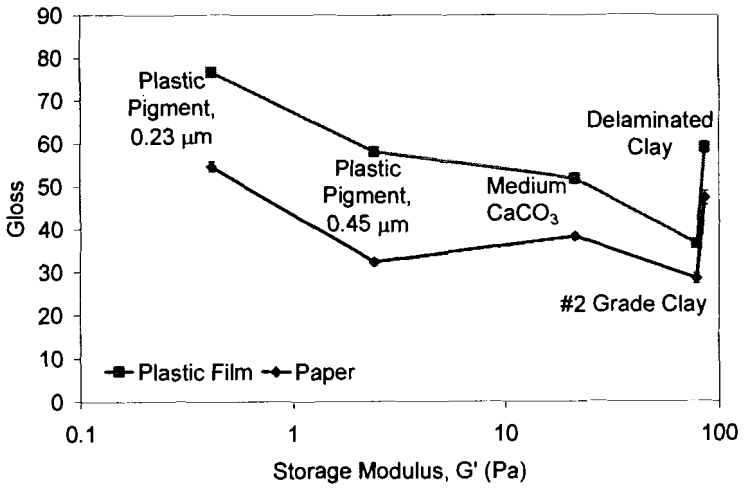

Figure 4.20 Gloss as a Function of Storage Modulus for Different Pigments

4.6. Summary of the CMC Experiments

The molecular weight and concentration of CMC does change the rheology of the suspensions and some of the coating characteristics. The viscosity and the storage modulus increase as the CMC concentration increases. The phase angle decreases with increasing CMC concentration, but this particular trend had no affect on the final coating structure. The particle size distribution and shape seem to have a change on the final coating structure more than the rheology.

5. EFFECT OF POLYMER TYPES

The influence of polymer type is reported in this chapter. Several purposes motivate this work: 1) to reproduce Nisogi *et al.* (1, 2) results for the HASE system; 2) how CMC compares to HASE in the same pigment system; and 3) to relate the rheology of a coating suspension to the final coating structure.

5.1. Difference of the Polymers

Carboxymethyl cellulose (CMC) is an anionic, cellulosic water-soluble polymer. It is produced by carboxymethylation of cellulose where the hydroxyl groups of cellulose are converted to sodium carboxymethyl groups. The amount of conversion is known as the degree of substitution (DS) where the DS is determined by the amount of glucose units are derivatized by carboxyl groups. Figure 5.1 illustrates a CMC polymeric chain with DS 0.75.

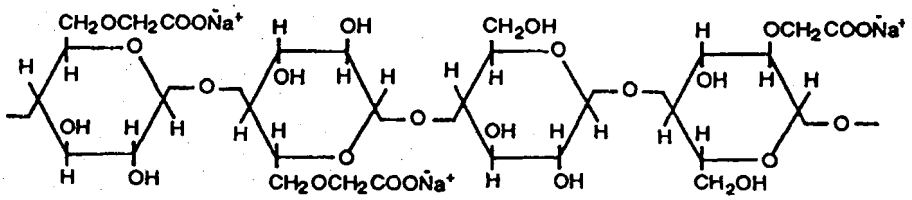

Figure 5.1 CMC with DS 0.75

Low DS results in poor water solubility properties, so CMC typically used for paper coatings has a DS range from 0.6 to 0.9. CMC is independent of pH and works well over a broad range of pH. It is a good film-forming agent and improves colloidal stability of a coating suspension. These properties help to achieve desired viscosities by inhibiting undesired shear thickening at high shear

rates. CMC also provides proper rheology, water retention and binder migration when used in correct proportion with the aqueous phase (62).

Hydrophobically modified alkali-swellable emulsion (HASE), an associative thickener, is an anionic hydrophobically modified polyacrylate synthetically derived from petroleum. This polymer is pH dependent so that as the pH increases, an electrostatic repulsion is created that causes the polymer chain to swell or dissolve. This allows interactions with water and acid groups in the aqueous phase. Figure 5.2 illustrates the polymer interactions of HASE before and after pH adjustment. Because of the shown interaction, HASE allows the coating suspensions to shear thin in response to stress and quickly regain viscosity for rapid immobilization (63).

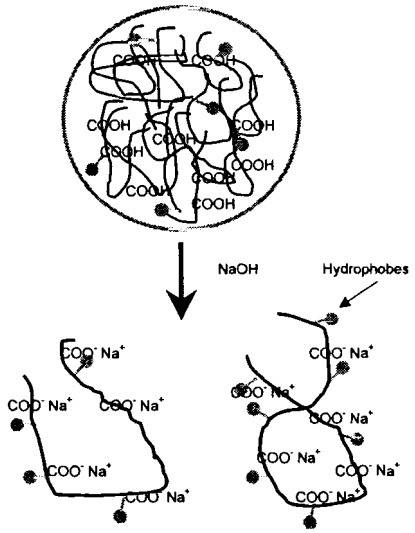

Figure 5.2 HASE Before and After pH Adjustment

Hydrophobically ethoxylated urethane (HEUR) is an associative thickener, like HASE, with a hydrophilic polymeric backbone. HEUR functions at low shear viscosities by intermolecular association interacting with the latex particles, Figure 5.3. For this reason, it is able to build low shear viscosity. When high shear is applied, the interactions break down giving way to low viscosity producing good runnability properties. HEUR is independent of pH, but its performance depends on the system (63).

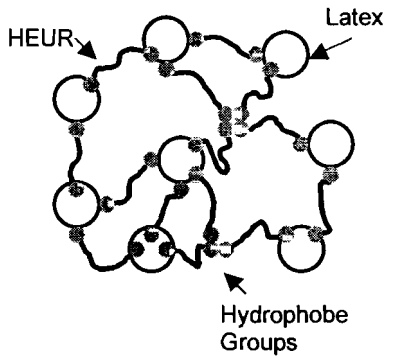

Figure 5.3 HEUR Interactions at Low Shear

From this discussion, it may be concluded that the HEUR has the weakest intermolecular forces followed by CMC then HASE. For the comparison of polymers, Table 5.1 shows the systems that were compared. All systems listed in Table 5.1 were compared at 60% solid by weight. The first system listed was used in this comparison for comparing these results with those of Nisogi *et al.* (1).

Table 5.1 Polymers Used

Pigment	Binder	Polymer
#2 Grade Clay	5 pph SB Latex (GenFlo 576, Omnova)	0.2 pph HASE
Delaminated Clay (D clay)	10 pph SB Latex (Dow CP 620NA)	0.1 pph HASE
		0.1 pph CMC
		0.1 pph HEUR

5.2. Rheological Comparison of Polymers

In all cases for this study, as the shear rate increases, the viscosity decreases indicating shear thinning for all polymers that were used, as seen in Figure 5.4. Comparing HASE in #2 grade clay and in the delaminated clay, the #2 grade clay sample seems to have a higher viscosity than that of the delaminated clay sample. This may be due to the higher concentration of HASE in the #2 grade clay (Table 5.1). HEUR, on the other hand, seems to have a lower viscosity than all other polymers, and this may be due to the breakdown in the intermolecular associations.

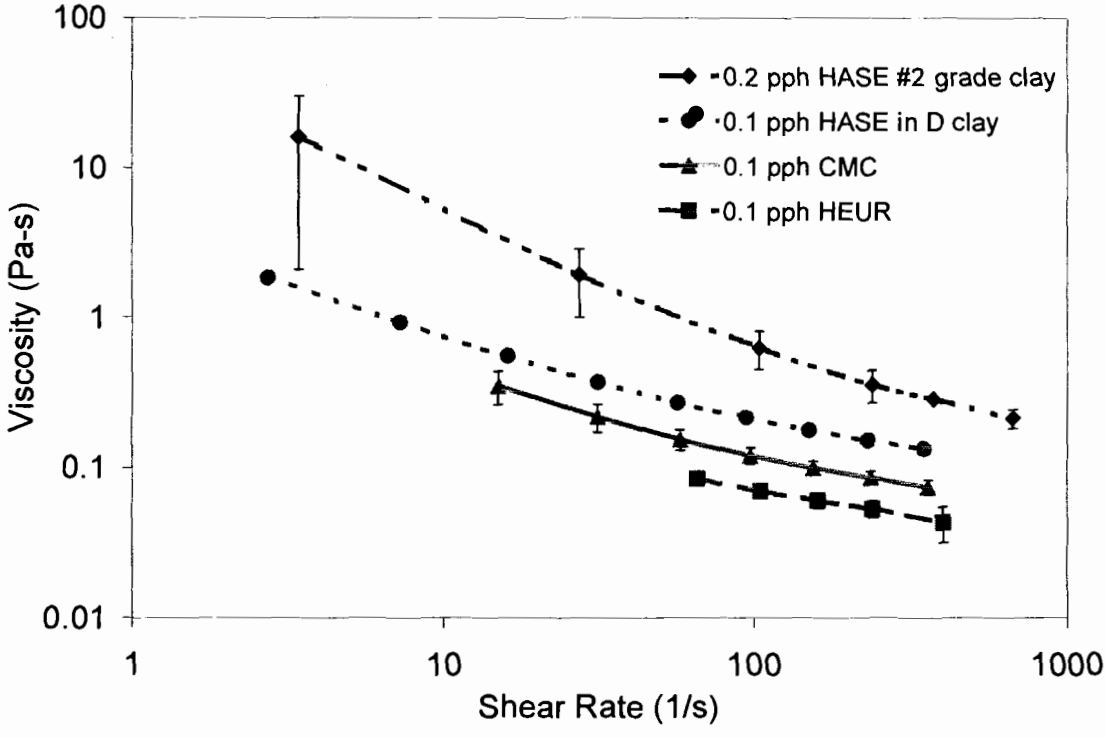

Figure 5.4 Steady Shear Viscosity for Polymer Comparison

As shown in Figure 5.5, the modules are plotted as a function of frequency. The HASE and CMC seem to behave in the same manner over a frequency of 0.5 to 5 Hz. The HEUR behaves differently in that, at a frequency of 3 Hz, the loss modulus, G", becomes dominant. Again, this may be due to the intermolecular associations completely breaking down. The collected data may be the viscosity of the aqueous layer and not that of the entire suspension. The 0.2 pph HASE system is quite elastic, with a storage modulus over one order greater than its loss modulus and the other storage modules.

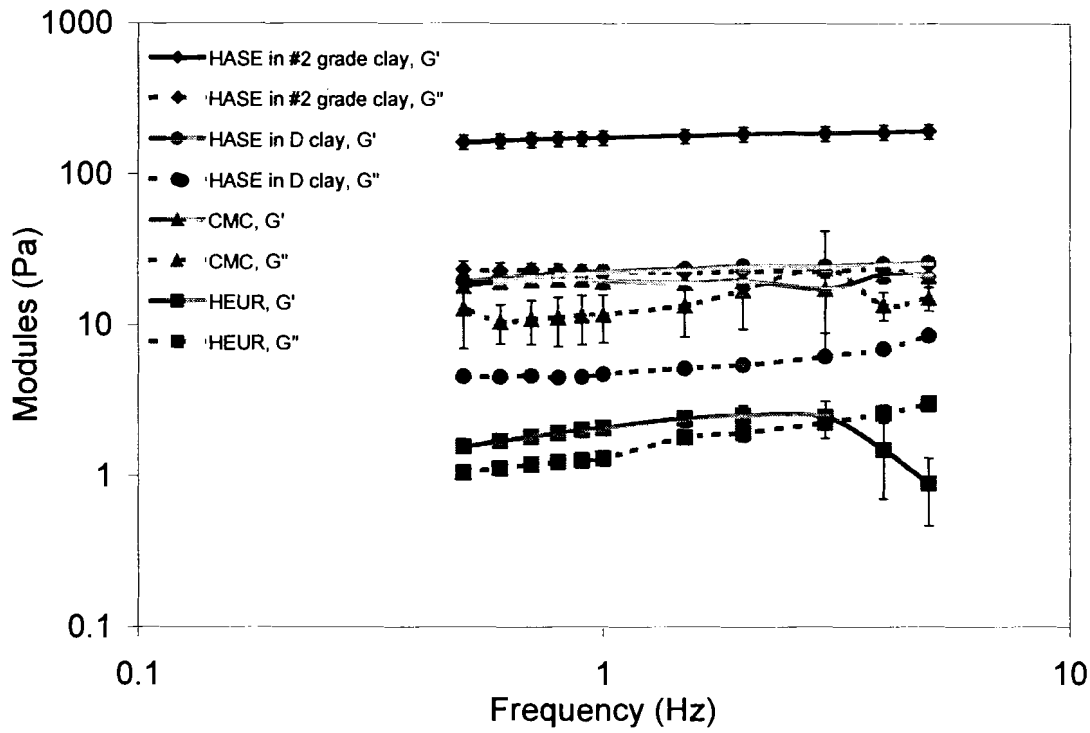

Figure 5.5 Oscillatory Measurement for Polymer Comparison for the Coatings in Figure 5.4

Figure 5.6 is a plot of the decreasing phase angle as a function of time, after a steady shear. HEUR possesses the highest phase angle compared to the other polymers tested, as seen in this figure. This behavior is due to the weak intermolecular interactions in this system. However, the presence of the phase angle around 30 degrees and decreasing indicates that, although the network may be weak, it still forms and is significant. The 0.2 pph HASE a phase angle less than 10 degrees indicating an elastic behavior.

CMC also seems to have similar behavior to HEUR indicating similar behavior as discussed above. Elasticity is present in the system, but does not appear to be as strong as the elasticity in the HASE systems. Nisogi *et al.* (2)

found that the HASE systems usually possessed a phase angle close to 10 degrees indicating the dominance of the elastic modulus, G', over the loss modulus, G". HASE in #2 grade clay has a lower phase angle than HASE in the delaminated clay. This is due to the polymer concentration (Table 5.1) in the #2 grade clay system. It is also important to note that the HASE in #2 grade clay line correlates with the results found by Nisogi *et al.* (2).

The slopes of these lines follow the logarithmic fit of Equation (3.1). Table 5.2 shows the values of this fit for these polymers. The final phase angle increases with decreasing viscosity (Figure 5.4) and intermolecular strength, and the slopes of these lines slightly decrease with decreasing viscosity and intermolecular strength.

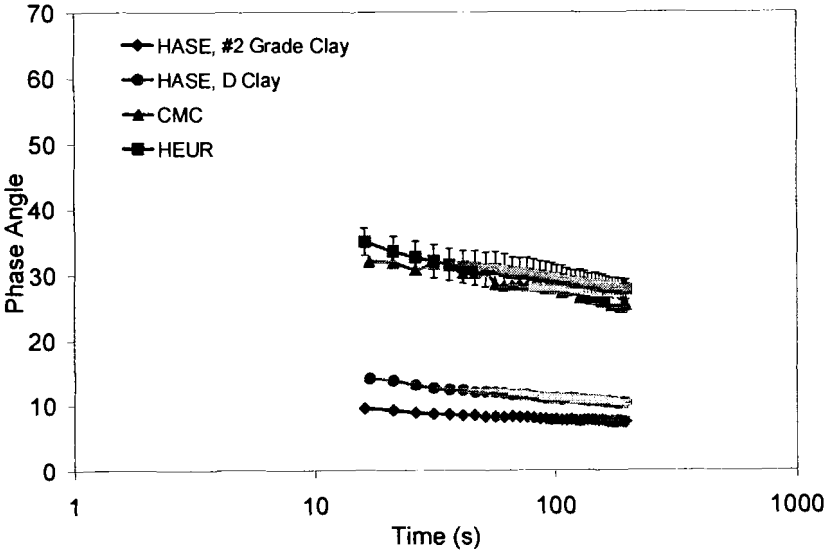

Figure 5.6 Phase Angle for Polymer Comparison for the Coatings in Figure 5.4

Table 5.2 Logarithmic Fit of Phase Angle and Time Relationship for Polymer Comparison

Phase Angle, δ	δ_{Final}	a	a/δ_{Final}	b	R^2
HASE, #2 grade clay	7.51	-0.75	-0.0999	11.35	0.9682
HASE, delaminated clay	10.39	-1.51	-0.145	18.10	0.9751
CMC, delaminated clay	25.67	-2.62	-0.102	29.34	0.9448
HEUR, delaminated clay	27.98	-2.32	-0.0829	40.24	0.9904

Figure 5.7 shows the storage modulus as a function of time after a steady shear. The HASE and CMC in delaminated clay seems to be similar in behavior, but the initial G' that is detected is lower in the case of CMC and regains at a faster rate to equal the final G' of HASE. Again, HEUR has a very low G' indicating structure breakdown due to stress.

The slopes of these lines follow the logarithmic fit of equation (3.2). Table 5.3 shows the values of this fit for these polymers. The final storage modulus increases with increasing viscosity (Figure 5.4) and intermolecular strength. However, the slopes of these lines do not change in the fashion as the phase angle. The CMC seems to reform slightly faster than the HEUR and HASE in delaminated clay.

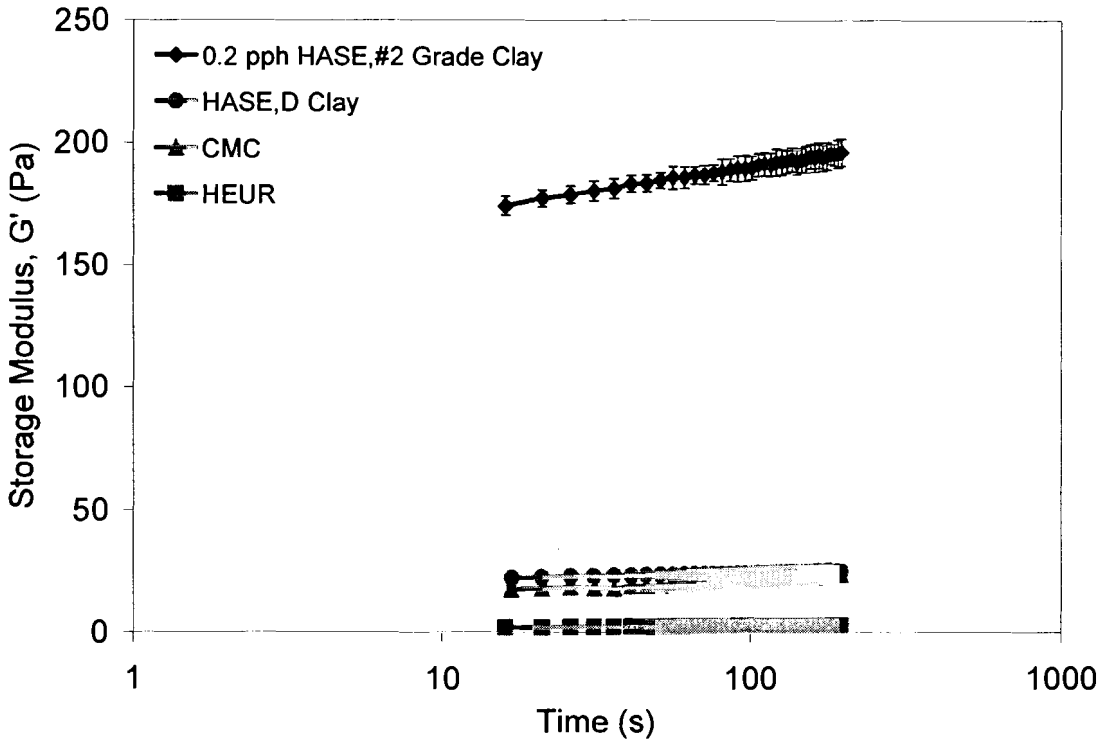

Figure 5.7 Storage Modulus Comparison of Polymers for the Coatings in Figure 5.4

Table 5.3 Logarithmic Fit of Storage Modulus and Time Relationship for Polymer Comparison

Storage Modulus, G'	G'_{Final}	a	a/G'_{Final}	b	R^2
HASE, #2 grade clay	194.77	8.31	0.0427	151.49	0.9958
HASE, delaminated clay	24.95	1.09	0.0437	19.31	0.9887
CMC, delaminated clay	23.32	1.92	0.0823	11.68	0.9911
HEUR, delaminated clay	2.77	0.30	0.1083	1.20	0.9986

5.3. Coating Characterization

Figure 5.8 shows that as the polymer concentration increases, the void fraction increases for all cases except CMC. The coat weight for all samples tested on plastic film was 33 ± 4 g/m^2. This indicates that although CMC provides coating elasticity, it has no affect on the final coating porosity. HASE and HEUR seem to build more coating structure than CMC. This may be due to the way the polymers associate with in the coating suspensions. This trend was also observed by Nisogi *et al.* (1) for HASE, and the values reported below are similar to those obtained by them.

A surprising result is that the HEUR, even though it has a low shear viscosity and a small storage modulus, gave a significant increase in void fraction. CMC has similar rheology to the HASE, but gives a negligibly increase in void fraction. There must be some mechanism, during drying, that causes CMC to behave differently that HASE or HEUR. Possibly, when water evaporates, the electrostatic interactions of CMC collapse while the hydrophobic interactions remain.

At Åbo Akademi (31, 61, 64), they found that for their systems of varying latex binder properties, no correlation between coating suspension elasticity and void fraction was found, but a correlation seemed present between the water retention of the suspension and the final coating structure.

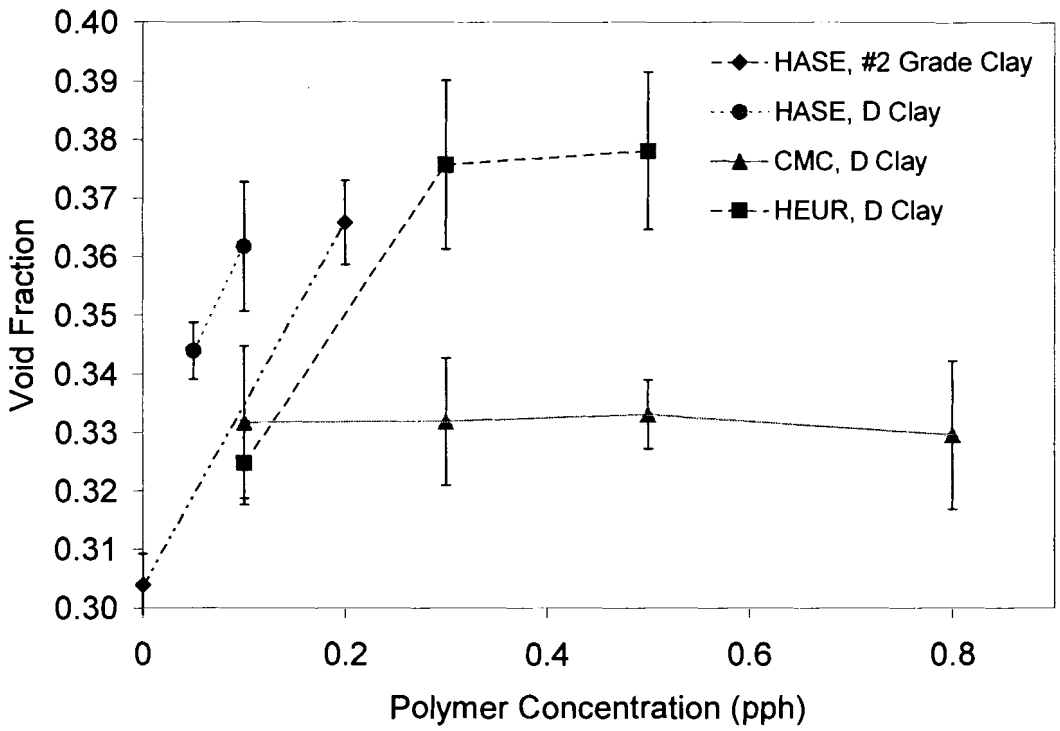

Figure 5.8 Void Fraction as a Function of Polymer Concentration for the Coatings in Figure 5.4

In Figure 5.9, water absorption is plotted as a function of polymer concentration on plastic film. As polymer concentration increases, water absorption also increases for the HASE and HEUR systems, which confirms the void fraction results. The absorption for CMC also confirms the void fraction results in that there is no increase in absorption as the polymer concentration increases. Overall, only the 0.2 pph HASE gave a significant increase in the absorption.

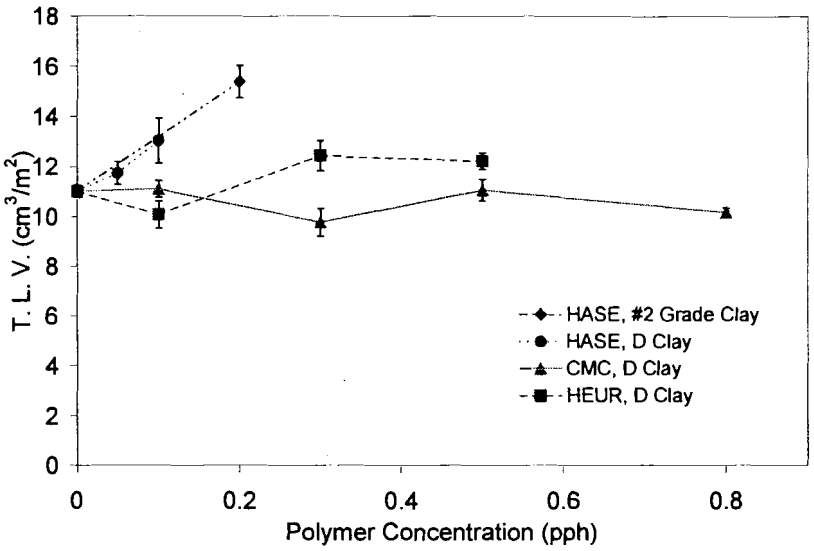

Figure 5.9 Water Absorption as a Function of Polymer Concentration for the Coatings in Figure 5.4

Figure 5.10 shows that gloss decreases with increasing polymer concentration. This would indicate more structured coatings that would produce rough coating surfaces resulting in lower gloss indicating a reduction in gloss due to poor leveling. This trend is small for the CMC system studied.

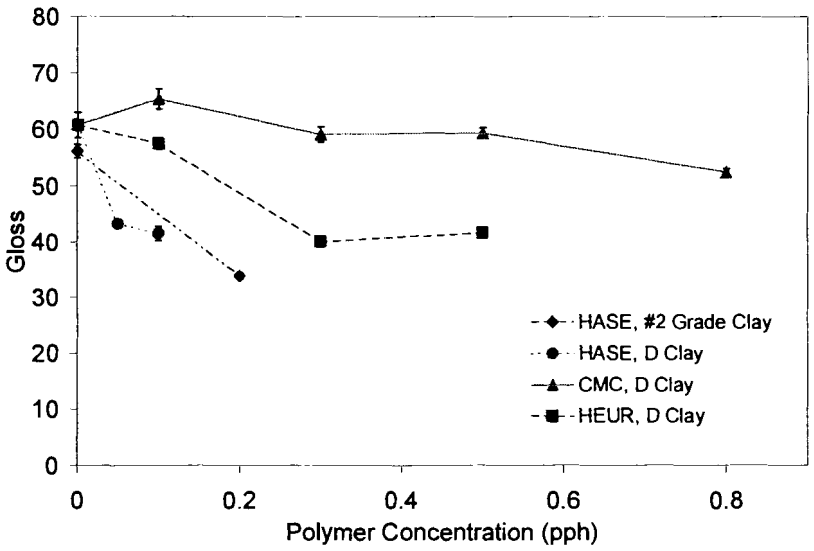

Figure 5.10 Gloss as a Function of Polymer Concentration for the Coatings in Figure 5.4

The light scattering coefficient is shown in Figure 5.11. As observed by Nisogi *et al.* (1), the light scattering coefficient (LSC) increases with increasing polymer concentration for the HASE and HEUR systems. The increase for the CMC system is present but small. As mentioned before in Chapter 3, the LSC is system dependent. Therefore, Figure 5.11 illustrates that HASE in #2 grade clay has lower LSC values than HASE in delaminated clay, but they follow the same trend. The CMC also appears to follow the same trend. This trend does not agree with the void fraction, water absorption, and gloss results, but the trend is weak. The HEUR gave the largest increase, even though it has the lowest viscosity and smallest storage modulus. The simple correlation given by Nisogi *et al.* between storage modulus and coating structure does not hold for all polymers.

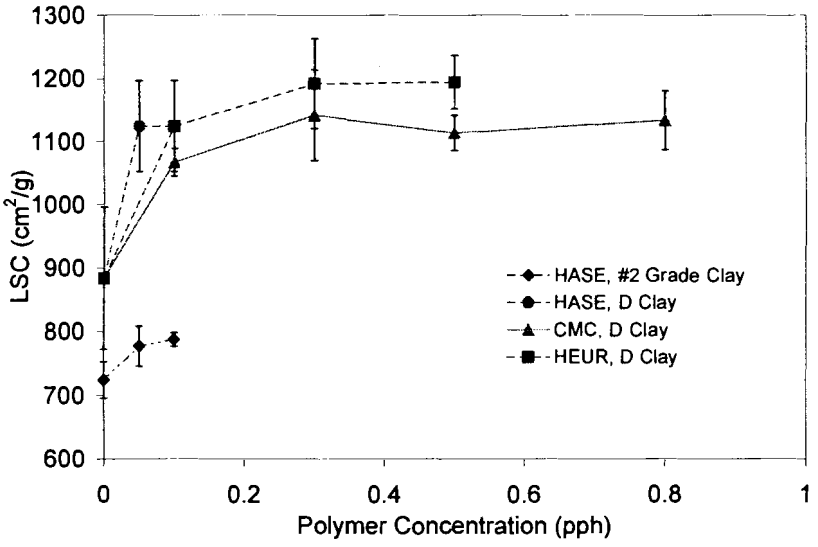

Figure 5.11 Light Scattering Coefficient as a Function of Polymer Concentration for the Coatings in Figure 5.4

5.4. Summary of the Polymer Comparison

Associative thickeners seem to have a significant affect on the dry coating characteristics, while the CMC has little influence. However, no general correlation could be made between the rheological measurements and the coating characteristics; HEUR had the lowest storage modulus but the largest influence on structure. The findings of Nisogi *et al.* (1, 2) were duplicated for that system. The increase in void fraction as a function of storage modulus only holds for each specific polymer.

6. COMPARISON OF APPLICATION METHODS

The coating suspensions were applied by means of a laboratory rod draw down coater, a cylindrical laboratory blade coater (CLC), and an internal-mixing air assisted spray coater as discussed in Chapter 3. The substrates used was 80 g/m^2 base weight wood free paper from Hansol Paper. The coat weight was adjusted to range from 20 to 150 g/m^2. Samples coated using the CLC were dried using IR heat at 25% drying capacity, and all other samples were dried at room temperature. The base line formulation of delaminated clay with 0.1 pph low molecular weight CMC was used for this study. Table 3.1 can be referred to for the coating formulation.

6.1. Rheological Experiments

Figure 4.1, a plot of the steady shear viscosity as a function of shear rate for the CMC molecular weight comparison, shows that the viscosity decreased slightly with increasing shear rate for the low molecular weight CMC sample. Figure 4.2, the oscillatory measurement as a function of shear rate for the CMC molecular weight comparison, shows the storage modulus dominance over the loss modulus for the frequency range of 0.5 Hz to 5 Hz. In Figures 4.3 and 4.4, the phase angle plot and storage modulus are plotted as a function of time after a steady shear for the CMC molecular weight comparison; the coating elasticity increased as a function of time.

6.2. Coating Characterization

The void fraction is compared to coat weight in Figures 6.1 and 6.2 for samples without CMC and with CMC, respectively. The CLC coated samples have a lower void fraction than the other application methods. This may be due to the IR drying technique that was used for the CLC coated samples. The high shear applied by the blade coater and the drying technique may not allow enough time for the structure to recover. On the other hand, the coating suspensions are subjected to high shear rates (10^6 s^{-1}) but these samples seem to have high voids. The coating may be drying when it mixes with the air as it hits the substrate. As discussed in Chapter 3, the void fraction of the base paper was subtracted out of the final void fraction by using equation (3.6). This subtraction may be an overestimation of the void fraction of the paper since the coating layer may penetrate into the paper voids, especially for the blade coated samples. Therefore, the low void fraction may be an artifact of the void fraction test.

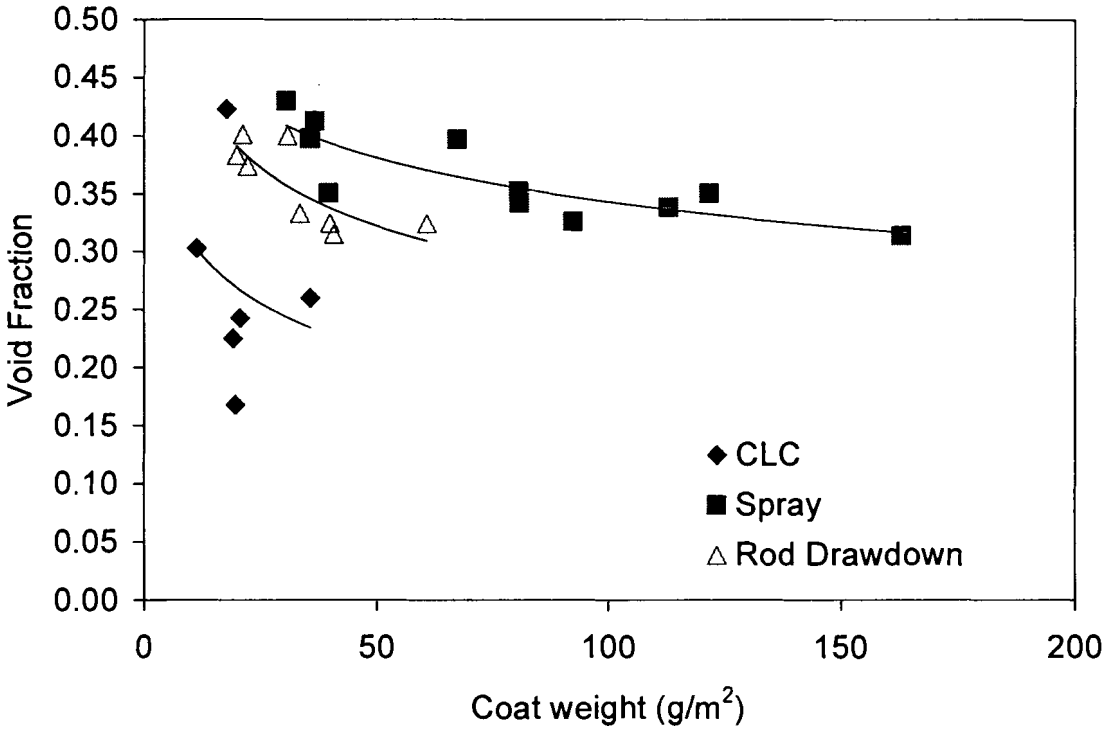

Figure 6.1 Void Fraction of Three Application Methods for No CMC Coatings on Paper as a Function of Coat Weight

When CMC is used, the void fraction is still a function of application method as seen in Figure 6.2. Even though the coat weight do not overlap in spray coating, the spray coated samples have a higher void fraction than the other application methods. A typical spray coated paper sample at 20 g/m^2 coat weight viewed at 5 times and 10 times of magnification by an optical microscope are illustrated in Figure 6.3.

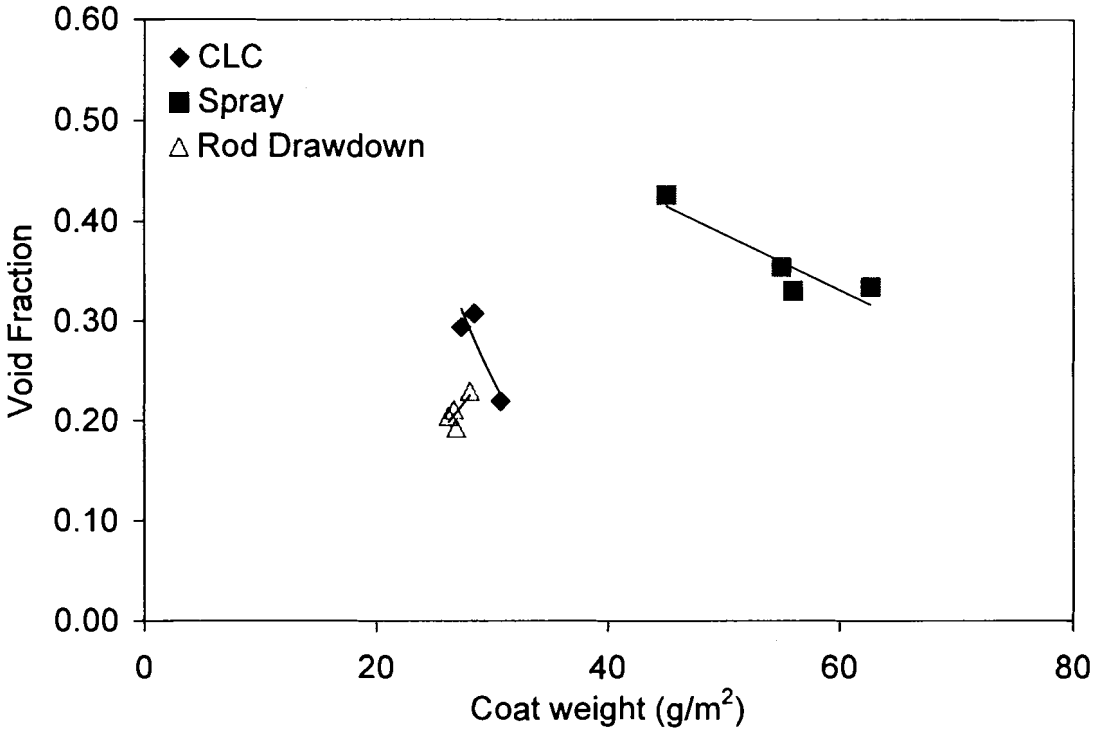

Figure 6.2 Void Fraction of Three Application Methods for CMC Coatings on Paper as a Function of Coat Weight

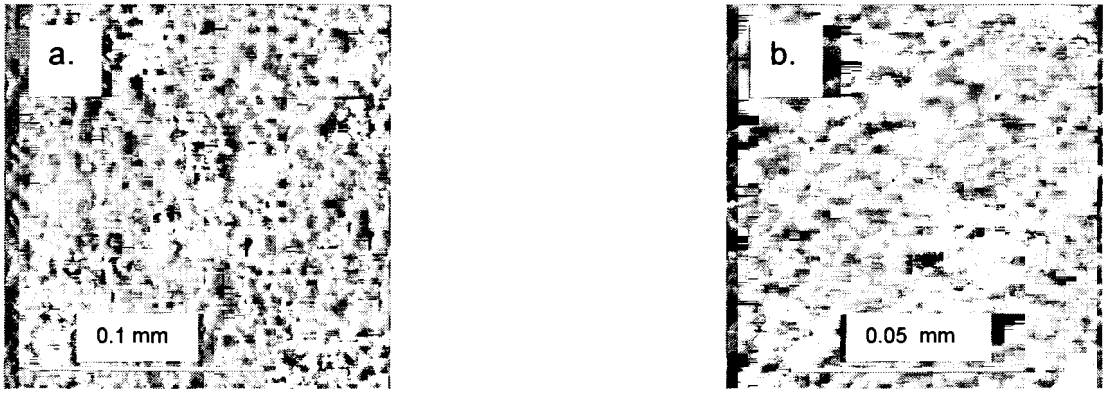

Figure 6.3 Spray Coated Samples Magnified at 5 Times (a.) and 10 Times (b.)

Figure 6.4 shows the water absorption as a function of coat weight for the coating containing CMC. The absorption is higher for the spray-coated samples. This is due to the uneven coating layer. The spray-coated samples have a much

higher absorption than the other paper samples because the uncoated portions of the paper may be absorbing the water at a faster rate than the evenly coated samples.

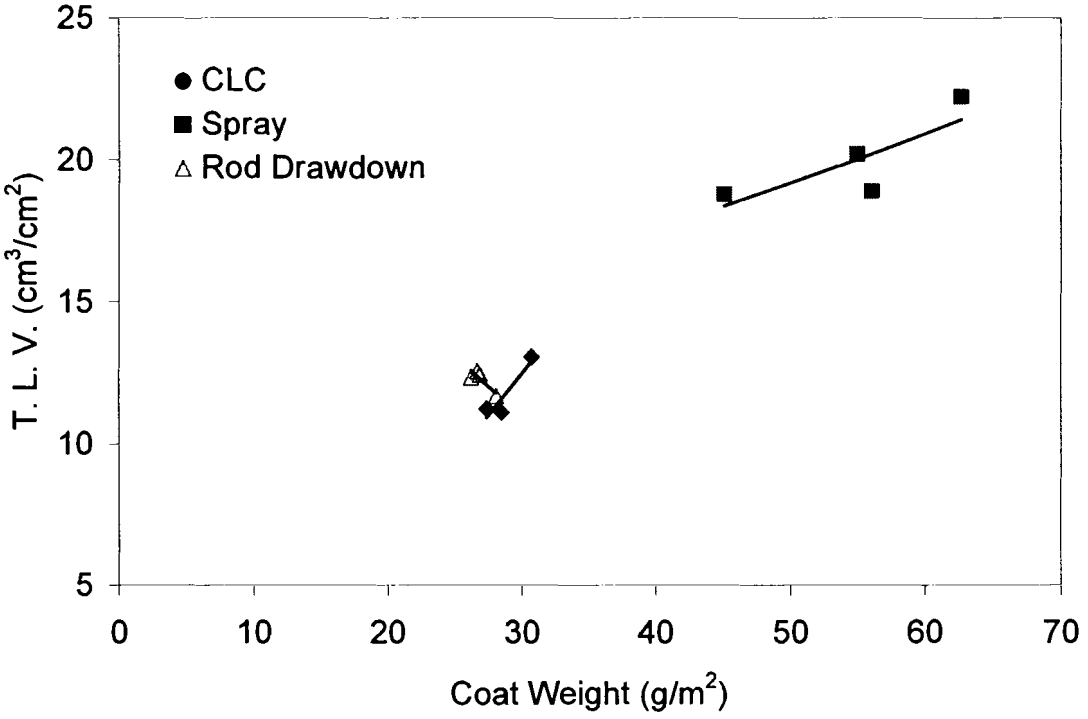

Figure 6.4 Water Absorption of Application Method Comparison for CMC Coatings on Paper as a Function of Coat Weight

Figure 6.5 illustrates the gloss as a function of coat weight for the different application methods. The spray coating method results in a lower gloss than the other application methods. Again, this is due to the amount of substrate coverage and non-uniformity of the coating layer. The rod coater and the CLC result in about the same gloss.

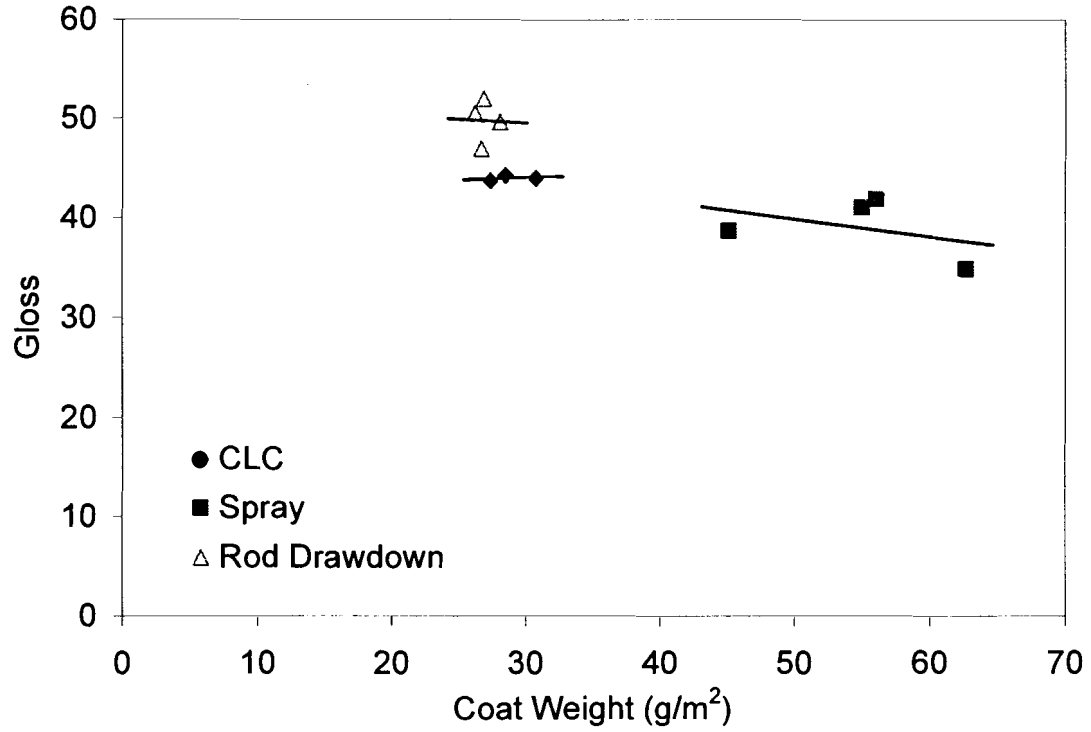

Figure 6.5 Gloss of Application Method Comparison for CMC Coatings on Paper as a Function of Coat Weight

In Figures 6.6 and 6.7, light scattering coefficient is considered as a function of application method for coatings not containing CMC and containing CMC, respectively. The spray-coated samples tend to have a lower LSC than the other application methods. When CMC is added to the system (Figure 6.7), the LSC seems to be affected only by the coat weight and not by the application method. Overall, the application method seems to have a small affect on the light scattering coefficient. This does not agree with the void fraction results that show spray coating with more voids.

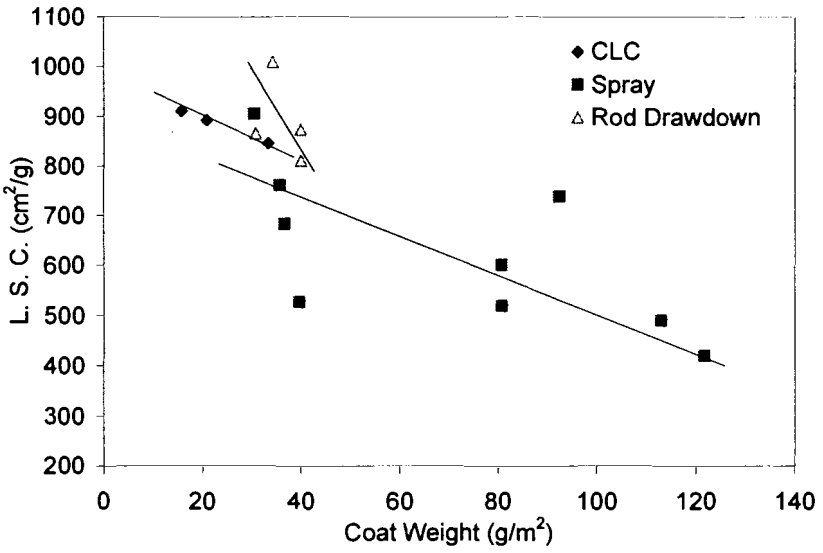

Figure 6.6 Light Scattering Coefficient for No CMC Coatings on Paper

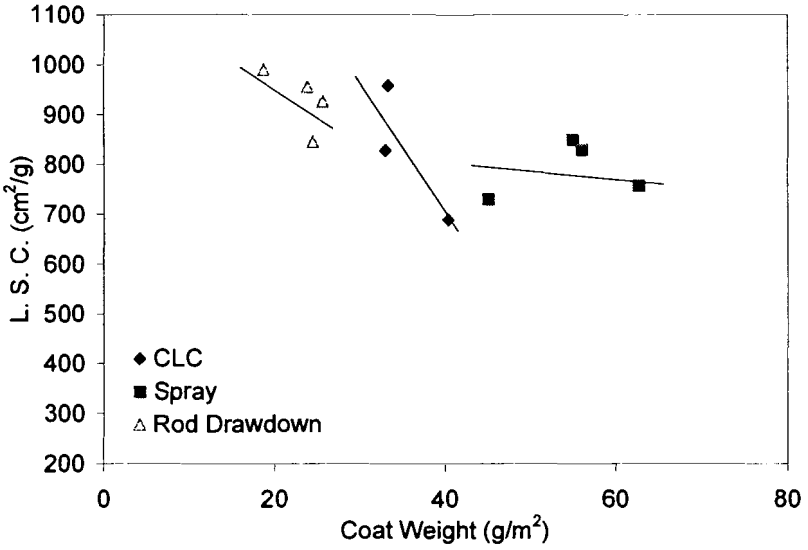

Figure 6.7 Light Scattering Coefficient for CMC Coatings on Paper

6.3. Summary of Application Methods

The void fraction, absorption, and gloss indicated that the spray coating method has higher void fraction, higher absorption rate, and a lower gloss than the other two methods. This is due to the surface roughness of the spray coated samples since the drops are not able to cover the surface in a uniform manner for these conditions. The light scattering coefficient was not a strong function of application methods.

7. CONCLUSIONS

The goals of this work were to determine if polymer additives or process conditions influence the final coating structure. A relationship between an increase in storage modulus and the final coating properties could not be made for the CMC containing suspensions, but for HASE suspensions, an increase in storage modulus resulted in an increase in voids. Therefore, only certain polymers that alter the rheology will also alter the final coating structure. The pigment shape, type, and size distribution had a stronger influence on structure than on the rheological behavior. Associative thickeners change the rheology and the final coating structure properties. Blade coating and rod coating have a small affect on the final coating structure; spray coating produces non-uniform coverage that results in high voids, high water absorption rates, and low gloss.

8. RECOMMENDATIONS FOR FUTURE WORK

Other important aspects of this work include looking at a broader range of molecular weights of CMC and exploring other molecular weights of CMC at different concentrations. This kind of study may give more of an insight on the adsorption behavior of CMC and the drying mechanism of coatings containing CMC. This kind of study may also give some insight into the difference between cellulosic thickeners and associative thickeners.

It would also be interesting to explore other polymers, such as HASE and HEUR, using the different application methods to determine if the same trends that were observed for CMC containing coatings exist for other polymers. The HEUR exhibits interesting rheological characteristics as related to the final coating structure for rod-coated samples, so the effect of different application methods would be interesting to explore.

As seen from the discussion on CMC concentration, the void fraction technique may not be an effective one for measuring porosity of a coating. It would be beneficial to develop a different, cost effective manner of measuring void fraction that would be easy to test and reproducible from one tester to another. The oil absorption technique does little to correct for the coating penetration into the paper substrate, so a more effect technique, other than mercury porosimetry, that would correct for this is essential to measure the coating porosity.

REFERENCES

1. Nisogi, H., Bousfield, D. W., and LePoutre, P., "Influence of Coating Rheology on Final Coating Properties," *Tappi J.*, 83(2), 100 (2000).
2. Nisogi, H., Bousfield, D. W., and LePoutre, P., "Influence of Dynamic Rheological Behavior on Final Coating Properties, Part 2 – Dynamic Suspension Rheology and Coating Structure Consolidation," *Tappi J.*, 83(5), 1 (2000).
3. Lavoie, P. A., Ghosh, T., and Carreau, P. J., "The Rheology of Coating Colors: A Comprehensive Approach," *1996 International Paper and Coating Chemistry Sym.*, 253 (1996).
4. Lavoie, P. A., Carreau, P. J., and Ghosh, T., "Rheology of Suspensions: The Flow Behavior of Coating Colors," *J. Pulp and Paper Sci.*, 23(11), J543 (1997).
5. Barnes, H. A., Hutton, J. F., and Walters, K., *An Introduction to Rheology*, Elsevier Science B.V., The Netherlands, 1989.
6. Sato, T., "Rheology of Suspensions," *J. Coating Technology*, 67(847), 69 (1995).
7. Fadat, G., Engström, G., and Rigdahl, M., "The Effect of Dissolved Polymers on the Rheological Properties of Coating Colours," *Rheological Acta*, 27, 287 (1988).

8. Persson, T., Järnström, L., and Rigdahl, M., "Effect of Method Preparation of Coating Colours on the Rheological Behavior and Properties of Coating Layers and Coated Paper," *1995 TAPPI Coat. Conf. Proc.*, TAPPI Press, Atlanta, 1995, p. 101.
9. Ghosh, T., "Rheological Measurement Techniques for Coating Colors, with Reference to Runnability," *1997 TAPPI Adv. Coat. Fund. Sym. Proc.*, TAPPI Press, Atlanta, 1997, p. 43.
10. Roper, J. A., and Attal, J. F., "Evaluations of Coating High Speed Runnability using Pilot Coater Data, Rheology Measurements, and Computer Modeling," *Tappi J.*, 76(5), 55 (1993).
11. Wilson, T. S., and Greenbalt, G. D., "Capillary Viscometry of Paper Coating Colors and Correlation to Coating Behavior," *Symposium on Coating Rheology*, ACS (1995).
12. McGenity, P. M., Gane, P. A. C., Husband, J. C., and Engley, M. S., "Effects of Interactions Between Coating Color Components and Rheology, Water Retention and Runnability," *1992 TAPPI Coat. Conf. Proc.*, TAPPI Press, Atlanta, 1992, p. 133.
13. Chonde, Y., Roper, J., and Salminen, P., "A Review of Wet Coating Structure: Pigment/Latex/Cobinder Interaction and its impact on Rheology and Runnability," *1995 TAPPI Adv. Coat. Fund. Sym. Proc.*, TAPPI Press, Atlanta, 1995, p. 57.
14. LePoutre, P., and Lord, D., "Destabilized Clay Suspensions: Flow Curves of Coating Colors," *J. Coll. Int. Sci.*, 134(1), 66 (1990).

15. Triantafillopoulos, N., and Grankvist, T. O., "Viscoelasticity and High Shear Coating in Relationship to Short-Dwell Runnability," *1992 TAPPI Coat. Conf. Proc.*, TAPPI Press, Atlanta, 1992, p. 23.

16. Triantafillopoulos, N., "High Speed Coating and Rheology," *AIChE Annual Meeting*, San Francisco (1994).

17. Carreau, P. J., and Lavoie, P. A., "Rheology of Coating Colors: A Rheologist Point of View," *1992 TAPPI Coat. Conf. Proc.*, TAPPI Press, Atlanta, 1992, p. 1.

18. Watanabe, J., and LePoutre, P., "A Mechanism for the Consolidation of the Structure of Clay-Latex Coatings," *J. Appl. Polym. Sci.*, 27(11), 4207 (1982).

19. LePoutre, P., "The Structure of Paper Coatings: An Update," *Prog. In Organic Coatings*, 17, 89 (1989).

20. Alince, B., and LePoutre, P., "Porosity and Optical Properties of Clay Coatings," *J. Coll. Int. Sci.*, 76(2), 439 (1980).

21. Lee, D. I., "Coating Structure Modification and Coating Hold-out Mechanisms," *1981 TAPPI Coat. Conf. Proc.*, TAPPI Press, Atlanta, 1981, p. 143.

22. LePoutre, P., "Substrate Absorbency and Coating Structure," *Tappi J.*, 61(5), 51 (1978).

23. Hemstock, G. A., and Bergmann, R. J., "Studies of Relationships Between Suspension and Paper Coating Film Properties. (1). Clay-Water Systems," *Tappi J.*, 51(11), 489 (1968).

24. Steinus, P., Kuortti, J., and Kronberg, B., "Competitive Adsorption Phenomena in Paper Coatings," *Tappi J.*, 67(5), 56 (1984).

25. Baumeister, M., and Kraft, K., "Quality Optimization by Control of Coating Structure," *Tappi J.*, 64 (1), 85 (1981).

26. Beck, U., Goossnes, J. W. S., Rahlwes, D., and Wallpott, G., "Coating Color Structure and Water Retention," *Proc. 1983 TAPPI Coat. Conf.*, TAPPI Press, Atlanta, 1983, p.47.

27. Lee, D. I., "Packing of Spheres and Its Effect on the Viscosity of Suspensions," *J. Paint Technology*, 42(550), 579 (1970).

28. Whalen-Shaw, M., "Protein-Pigment Interactions for Controlled Rotogravure Printing Properties, Mechanic and Structural Considerations," *Proc. 1984 TAPPI Coat. Conf.*, TAPPI Press, Atlanta, 1984, p. 11.

29. Jarnström, L., Ström, G., and Stenius, P., "Adsorption of Dispersing and Thickening Polymers and their Effect on the Rheology of Coating Colors," *Tappi J.*, 60(9), 101 (1987).

30. Oittinen, P., "Interactions Between Coating Pigments and Soluble Binders in Dispersions," *Proc. 1981 TAPPI Coat. Conf.*, TAPPI Press, Atlanta, 1981, p. 113.

31. Backfolk, K., Grankvist, T., and Eklund, D., "The Effect of Binder Chemistry on the Colloidal Stability of Calcium Carbonate Suspensions," *2001 TAPPI Adv. Coat. Fund. Sym. Proc.,* TAPPI Press, Atlanta, 2001, p. 149.

32. Baumeister, M., "Morphology of Coatings Containing Polyvinyl Alcohol," *Wochbl. Papierfabr.*, 104(20), 769 (1976).

33. Sandas, S. E., and Salminen, P. J., "Pigment-Cobinder Interactions and Their Impact on Coating Rheology, Dewatering, and Performance," *Tappi J.*, 74(12), 179 (1991).

34. Climpson, N. A., and Taylor, J. H., "Pore Size Distribution and Optical Scattering Coefficients of Clay Structures," *Tappi J.*, 59(7), 89 (1976).

35. Bessho, N., and Ichikawa, A., "Study of Coating Layers with Various Styrene-Butadiene Latexes - Porosity and Rotogravure Printing," *Wochbl. Papierfabr.*, 114(20), 823, (1986).

36. LePoutre, P., and Rezanowich, A., "Optical Properties and Structure of Clay-Latex Coatings," *Tappi J.*, 60(11), 86 (1977).

37. Gate, L., Windle, W., and Hine, M., "Relationship Between Gloss and Surface Microstructure of Coatings," *Tappi J.*, 56(3), 61 (1973).

38. Gate, L. F., Highman, V. M., and Hine, M. J., "Reflection of the Surface of Matte-Coated Papers," *Papeterie*, 96(12), 823 (1974).

39. Isoard, J., "Ink Transfer and Retransfer: Mottling and Offset Picking of Coated Papers," *Proc. 1983 TAPPI, Coat. Conf.*, TAPPI Press, Atlanta, 1983, p. 143.

40. LePoutre, P., and De Grace, J. H., "Ink Transfer Characteristics and Coating Structure," *Paper Technol. Ind.*, 19(9), 301, (1978).

41. Trader, D., "Laboratory Studies Relating Coating Structure and Coating Performance," *Tappi J.*, 54(10), 1709 (1971).

42. Walter, J. C., *The Coating Processes*, TAPPI Press, Atlanta, 1993, p. 71-131.

43. Adolfsson, M., Engström, G., and Rigdahl, M., "The Effect of the Relaxation Time of Coating Colours on the Elimination of Blade Streaks," *1989 TAPPI Coat. Conf. Proc.*, TAPPI Press, Atlanta, 1989, p. 55.

44. Iliopoulos, I., Parish, T. D., and Scriven, L. E., "An Application of CFD to Blade Erosion by Particle Impact in Suspensions Coating," *2001 TAPPI Adv. Coat. Fund. Sym. Proc.*, TAPPI Press, Atlanta, 2001, p. 359.

45. Bousfield, D. W., Rigdahl, M., and Wikström, M., "Roll Deformation during Blade Coating," *Tappi J.*, 81(5), 207 (1998).

46. Kline, J. E., "The Dynamics of Blade Coater Rheology," *1985 TAPPI Coat. Conf. Proc.*, TAPPI Press, Atlanta, 1985, p. 181.

47. Bousfield, D. W., Isaksson, P., and Rigdahl, M., "Particle Motion Analysis at the Exit of a Blade Coater," *J. Pulp and Paper Sci.*, 23(6), 293 (1997).

48. Hull, M., "Visualization of Wire Wound Rod Coating Defects," *1990 TAPPI Polymers, Laminations & Coatings Conf.*, TAPPI Press, Atlanta, 1990, p. 539.

49. Hanumanthu, R., and Scriven, L. E., "Coating with Patterned Rolls and Rods," *1995 TAPPI Coat. Fund. Sym. Proc.*, TAPPI Press, Atlanta, 1995, p. 109.

50. Triantafillapoulos, N., Grön, J., Luostarinen, I., and Paloviita, P., "Operational Issues in High Speed Curtain Coating of Paper," *2001 TAPPI Coating and Graphic Arts Conf. Proc.*, TAPPI Press, Atlanta, 2001, p. 251.

51. "Convention Challenged: Traditional Coating Techniques Could Find Themselves Under Threat," *Pulp & Paper Europe* [online], Aug/Sept 2001. Available from: http://www.paperloop.com/. Accessed Auq 31, 2001.

52. MacLeod, D. M., Fahrendorf, P. M., "Rod Coating Comes of Age," *1988 TAPPI Polymers, Laminations & Coatings Conf.*, TAPPI Press, Atlanta, 1988, p. 203.

53. Lefebvre, A. H., *Atomization and Sprays*, Taylor & Francis, Levittown, PA, 1989, p. 10.

54. Hanumanthu, R., and Scriven, L. E., "Coating with Patterned Rolls and Rods," *1995 TAPPI Coat. Fund. Sym. Proc.*, TAPPI Press, Atlanta, 1995, p. 109.

55. Eklund, R. W., LeBlanc, H. A., and Halley, D. G., "CLC – A New High Speed Blade Coater for the Laboratory," *Tappi J.*, 71(12), 55 (1988).

56. Bristow J.A., "Liquid Absorption into Paper during Short Contact Time Intervals," *Svenk Papper Stidning*, 70(19), 623 (1967).

57. HunterLab Modular Glossmeter, Model D48-7, Instruction Manual.

58. Technidyne Corporation, "Technibrite Micro TB-1C Brightness, Opacity, Color, and Fluorescence Tester Instructional Manual," New Albany, IN.

59. Biermann, C. J., *Handbook of Pulping and Papermaking*, Academic Press, San Diego, 1996, p. 502-508, 514-515.

60. Zauscher, S., and Kingenberg, D. J., "Surface and Friction Forces between Cellulose Surfaces Measured with Colloidal Microscopy," *Nordic Pulp and Paper Research J.*, 15(5), 459 (2000).

61. Rousu, S., Grankvist, T., and Eklund, D., "The Effect of Polymers on the Final Coating Structure," *2001 TAPPI Adv. Coat. Fund. Sym. Proc.,* TAPPI Press, Atlanta, 2001, p. 149.

62. Kane, R. J., *Paper Coating Additives*, TAPPI Press, Atlanta, 1995, p. 28-34.

63. Rohm and Hass Company, "Rheology Modifiers and Dispersants: Specialty Polymers for Paper and Paperboard," (May 1997).

64. Kokka, A., Grankvist, T., and Eklund, D., "Physical and Chemical Modifications in Latex Binders and Their Effect on the Coating Color Rheology," *2001 TAPPI Adv. Coat. Fund. Sym. Proc.,* TAPPI Press, Atlanta, 2001, p. 171.

BIOGRAPHY OF THE AUTHOR

Basant Dimetry was born in Fayetteville, North Carolina on June 8, 1976. She was raised in Hinesville, Georgia where she graduated with honors from Bradwell Institute in June 1994 after completing a study abroad. She graduated from Georgia Southern University in June 1998 with a Bachelor's of Science in Chemistry. She began her career at Union Camp Corporation in June 1998 as a Product Development Laboratory Technician. When Union Camp became International Paper, she left the company in August 1999 to obtain a graduate degree at the University of Maine.

After receiving her degree, Basant will be seeking employment to begin her career in the field of coating suspensions. Basant is a candidate for The Master of Science degree in Chemical Engineering at The University of Maine in December, 2001.